J. Fluid Mech. (1995), *vol.* 292, *pp.* 153–182

Stationary perturbations of Couette–Poiseuille flow: the flow development in long cavities and channels

By JENNIFER R. STOCKER AND PETER W. DUCK
Department of Mathematics, University of Manchester, Manchester M13 9PL, UK

(Received 28 May 1994 and in revised form 10 January 1995)

We consider stationary perturbations to Couette–Poiseuille flows. These may be considered to be related to far downstream/upstream entry/end effects in flow inside long cavities and channels. Three distinct classes of basic flow are considered, all of which are exact solutions of the Navier–Stokes equations. We first study the problem in the case of Poiseuille flow, and are able to explain a previous discrepancy between fully numerical results, and asymptotic theory valid for large Reynolds numbers, R. The second case, which may be derived from a combination of an imposed streamwise pressure gradient and sliding of the upper channel wall, is for the particular situation where the flow on the lower surface is on the verge of reversing direction. The third case is relevant to the flow inside a long driven cavity (with closed ends, no imposed streamwise pressure gradient and no net mass flux). The flow is driven exclusively by a sliding top wall and mass conservation demands that the flow is no longer unidirectional.

For low Reynolds numbers, the stationary eigenvalues in all cases considered are complex (and hence are not monotonic in the streamwise direction). Indeed as $R \to 0$ the eigenvalues become completely independent of the base profile. As the Reynolds number is increased, the eigenvalues generally undergo a number of branching processes switching between being complex and real (and vice versa) in nature, and at large Reynolds numbers fall broadly into three distinct categories, namely $O(1)$, $O(R^{-1/7})$ and $O(1/R)$. In this limit the eigenvalues may be either complex or real (tending to monotonic eigensolutions in the streamwise direction).

Of particular interest are certain of the $O(1)$ eigensolutions for the 'driven-cavity' problem, in the high-Reynolds-number limit; these turn out to be highly oscillatory (WKB-type) over much of the cavity section.

In all three cases, we use a combination of numerical and asymptotic techniques, and a thorough comparison between results thus obtained is made.

1. Introduction

The general class of problem considered is that of two-dimensional incompressible viscous flow through a long straight channel, with particular (but not exclusive) attention on the limiting case of high-Reynolds-number flow. Stationary small-amplitude perturbations to the fully developed flow in three different cases are investigated. The first case considered is that of plane Poiseuille flow, where both walls of the channel are stationary, with the flow driven exclusively by a uniform imposed pressure gradient. In the past, this case has been quite widely studied, both analytically and numerically. The disturbances to the basic flow are governed by a form of the

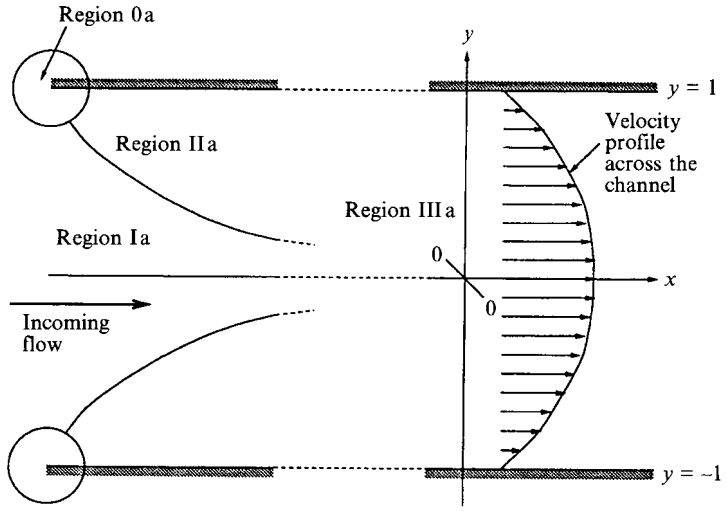

FIGURE 1. Plane Poiseuille flow in a channel.

Orr–Sommerfeld equation, and thus in general a numerical approach must be adopted. The previous numerical work on this particular problem includes that of Bramley & Dennis (1982, 1984) and Bramley (1984), who used a Chebyshev polynomial representation of the eigensolutions as the basis for their studies. One of our (two) numerical schemes is based on this method, and this previous work provides an extremely useful benchmark, and confirmed the integrity of our schemes. Additionally, for the case of plane Poiseuille flow, we present somewhat more comprehensive results than before, detailing results for many modes, over a range of Reynolds numbers. The problem is also tackled using asymptotic analysis valid for large and small Reynolds numbers, following Wilson (1969). We are also able to point out a slight inconsistency in this work.

The second case we consider is that of stationary perturbations to a linear combination of Couette and plane Poiseuille flows, generated by both an imposed streamwise pressure gradient and a moving top wall, for the special case when the shear on the (stationary) lower wall vanishes. Finally, the case of flow where the upper wall is moving, but there is no net mass flux (and no streamwise pressure gradient) in the fluid is considered, corresponding to flow inside a long 'driven' cavity.

Incompressible viscous flow through a channel is a widely studied problem. Various regions in the channel must be considered separately when attempting to solve the problem at large Reynolds numbers. The problem of flow entering the channel, with both the upper and lower plate fixed, i.e. plane Poiseuille flow development, has been studied by Van Dyke (1970) and Wilson (1971), and these studies correspond to our first case where the far downstream cross-sectional profile in the channel is a small perturbation to plane Poiseuille flow (see region IIIa in figure 1). Region Ia is an inviscid core, where the flow has not yet been affected by entry into the channel. Region IIa is where a Blasius-type boundary layer is forming. The region immediately adjacent to the leading edge of the plates – region 0a – is one in which the boundary-layer expansions are not valid, and the full Navier–Stokes equations describe the flow. These solutions can, in principle, be matched together to give an analytic approximation to flow in the entire channel.

Our second case is of less interest physically, but represents a mathematical

watershed. The conditions to which this case corresponds are flow through a channel with a moving lid, an overall mass flux, subject to an (adverse) pressure gradient, with flow that is on the verge of reversing on the lower wall.

The third case corresponds to flow through a long thin 'driven' cavity, with no imposed pressure gradient. This flow is subject to a mass restriction condition which leads to a parabolic cross-sectional profile and, interestingly, flow reversal far from the ends of the cavity. The work presented here is a consideration of flow in region IIIc in figure 2. Region Ic involves a corner where there probably exists an infinite sequence of alternately rotating eddies. The presence of these was shown by Moffatt (1964) for flow past a 'corner' of internal angle $\leqslant 146.3°$. Moffatt showed the presence of these eddies for low Reynolds numbers, but they have also been found numerically at higher Reynolds numbers. There is also a singularity in the flow in region 0c, where the moving lid meets the fixed wall. Flow reversal must take place in region IIc. Once again, separate (but matching) asymptotic descriptions are necessary for all of these regions. This case is particularly important from a physical perspective, because of the reversing nature of the flow. One goal of the paper is to glean some insight into the flow reversal process; indeed, some of our results for this particular case at high Reynolds numbers indicate some novel and intriguing complex features of the flow.

These stationary perturbations to the flow field may be produced in a variety of ways. One mechanism would be through endwall and entry flow effects, such as suggested in figures 1 and 2. Close to these locations disturbances must be large, but further away disturbances are expected to decay away, leaving just a basic flow (which may be taken to be independent of the streamwise location). The manner in which this state is approached will be determined to a large extent by the stationary eigensolutions. Alternatively, any flow distortion, such as a fixed obstacle located anywhere in the flow field or any steady perturbation of the boundary would also trigger such eigensolutions, both upstream and downstream of the perturbation. The work of Dennis & Smith (1980) is relevant here, in the context of perturbations to plane Poiseuille flow. Since the present work is concerned with locations distant from the actual flow perturbation, we assume that the disturbances have decayed sufficiently and so there is no need to impose any magnitude constraints on the source of the disturbances, *per se*, merely that the distance from the source of the distortion should be sufficiently large, so that the perturbations themselves are sufficiently small.

Previous work by one of the authors, Stocker (1992), describes a numerical scheme to solve the full, small-amplitude equations for any developed flow/cross-sectional profile. The results thus obtained both inspired and guided the following work. Our approach to these problems is similar to that for the first problem, namely the dual study using a combination of numerical and asymptotic techniques.

In spite of the fundamental nature of this general case of basic flow, it has received surprisingly little attention in the past (except, of course, for the two particular examples of Couette flow and plane Poiseuille flow), although Cowley & Smith (1985) did present some aspects of the associated stability analysis, but focused on the configuration where the wall was sliding in the same direction as the main body of the flow. The general basic flow and perturbation equations are derived in §2; our numerical schemes are described in §3. In §4 the particular case of plane Poiseuille flow is investigated, and our results are compared to previous analysis and numerical work. The second case (with the flow at the lower wall on the verge of reversing) is considered in §5, whilst in §6 the conditions pertinent to the long driven-cavity case are described. Our conclusions are given in §7. In the Appendix, the effects of small amounts of slippage (of either of the channel walls) on a particular class of eigensolutions for the

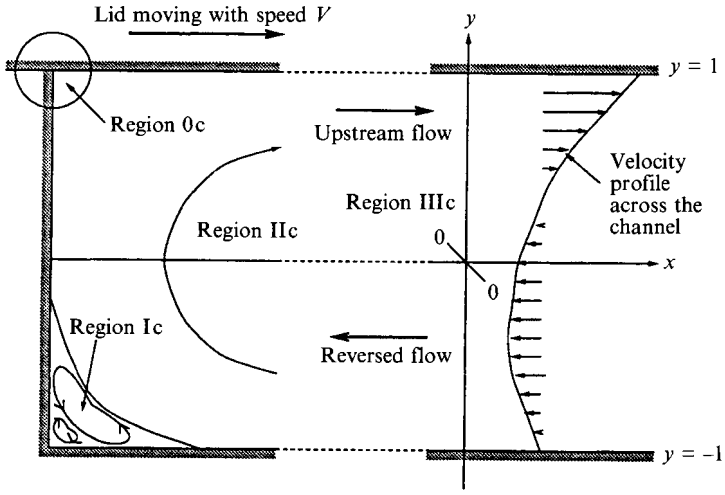

FIGURE 2. Flow in a long driven cavity.

plane Poiseuille flow problem is investigated, and confirms (and indeed sheds more light on) some of the observations found in the paper.

2. Formulation of the problem

We consider the two-dimensional flow through a long straight channel of width $2l$, with U_∞ being a representative velocity scale, and ν is the kinematic viscosity of the fluid (assumed constant). We take (lx, ly) to be the coordinate system, with $x = 0$ lying at some arbitrary location (for example the position of the channel entry or of the cavity wall), and $y = 0$ lying along the centreline of the channel, and so the walls are located at $y = \pm 1$. The Reynolds number is then defined to be

$$R = U_\infty l/\nu. \tag{1}$$

We take the dimensional velocity vector to be $U_\infty \boldsymbol{u}$ with $\boldsymbol{u} = (u, v)$, and pressure to be $\rho U_\infty^2 p$, where ρ is the fluid density (also assumed constant).

The non-dimensional form of the Navier–Stokes and continuity equations are then written

$$\frac{\mathrm{D}\boldsymbol{u}}{\mathrm{D}t} = -\nabla p + \frac{1}{R}\nabla^2 \boldsymbol{u}, \tag{2}$$

and

$$\nabla \cdot \boldsymbol{u} = 0. \tag{3}$$

On account of the two-dimensional nature of the flow, we find it convenient to introduce a stream function $\Psi(x, y)$, defined in terms of the velocity vector $\boldsymbol{u} = (\partial\Psi/\partial y, -\partial\Psi/\partial x)$. Equations (2) and (3) above may then be combined, and written in the following form (assuming the solution to be independent of time):

$$\frac{\partial(\nabla^2\Psi, \Psi)}{\partial(x, y)} = \frac{1}{R}\nabla^4\Psi. \tag{4}$$

We now consider the base flow in the channel. A general flow driven by a constant streamwise pressure gradient, together with an upper boundary ($y = 1$) moving

tangentially with speed V and a stationary lower boundary ($y=-1$) yields the following exact, general solution to (4):

$$\Psi_0(y) = \tfrac{1}{4}[V(y^3+y^2-y)+\gamma(3y-y^3)]. \tag{5}$$

This corresponds to flow with a mass flux of γ per unit width.

Following Wilson (1969), Bramley & Dennis (1982, 1984) and Bramley (1984), we now seek steady perturbations to this solution, by assuming a stream function of the form

$$\Psi(x,y) = \Psi_0(y)+[\phi(y)\exp(-\alpha x)+\text{c.c.}], \tag{6}$$

where c.c. denotes the complex conjugate. Here we assume $\phi(y)$ is $O(1)$, in general, and that $|x| \gg 1$; the constant α is an eigenvalue determining the decay of the perturbation, which may be real or complex. The determination of the values of α is the main focus of attention of this paper. Since we assume that $|x| \gg 1$, the perturbation term is relatively small compared to the base solution. The smaller $|\text{Re}(\alpha)|$ the further upstream/downstream any end effects are transmitted (where $\text{Re}(\alpha)$ denotes the real part of α). Substituting (6) into (4), and neglecting terms $O(\exp(-2\alpha x))$ leads to the following equation:

$$\phi^{\text{iv}}+2\alpha^2\phi''+\alpha^4\phi+\alpha R\left[\frac{\partial \Psi_0}{\partial y}(\phi''+\alpha^2\phi)-\frac{\partial^3 \Psi_0}{\partial y^3}\phi\right] = 0. \tag{7}$$

The appropriate boundary conditions are entirely homogeneous, and are those of impermeability and of no slip, namely

$$\phi(\pm 1) = \phi'(\pm 1) = 0. \tag{8}$$

The system (7) represents an eigenvalue problem for α, and may be regarded as a stationary (steady) Orr–Sommerfeld system. Viewed in an alternative way, (6) may be regarded as being the Laplace transform of the (perturbed) flow field; then poles in transform (α) space are directly related to the location of eigensolutions of the homogeneous problem. These poles will then be responsible, to a large extent, for determining the $|x| \gg 1$ nature of the flow. The inversion of the transformed solution from α- to x-space involves an integration in α-space. For $x > 0$, this must be carried out entirely in $\text{Re}(\alpha) > 0$, and for $x < 0$, this must be carried out entirely in $\text{Re}(\alpha) < 0$. Values of $\text{Re}(\alpha) > 0$ constitute solutions valid downstream of some flow event, whilst values of $\text{Re}(\alpha) < 0$ represent solutions valid upstream of some flow event; therefore the perturbation quantity determines to a large extent the manner in which the base flow solution is approached. Related arguments (albeit in the context of Fourier transforms) have been elucidated by Bogdanova & Ryzhov (1983) and Duck (1985), whilst a clear application and occurrence of stationary eigenmodes is to be found in the channel flow work of Dennis & Smith (1980).

In general, the system (7), (8) requires a numerical approach, and we consider the numerical schemes used in the following section.

3. Numerical methods

Two very different numerical schemes were employed in this study – a local iterative scheme, and a global method. The local scheme was based on a fourth-order Runge–Kutta method, which required an initial 'guess' for the eigenvalue, followed by Newton iteration in order to determine the correct value for α. The advantages of this scheme were that it was easy to program, and used very small amounts of storage space

and computing time. However, this approach only yields one solution per calculation, sometimes making it difficult to build up an overall picture of solution space. Also, problems were encountered with convergence, particularly when the Reynolds number was large, and when computing complex eigenvalues.

The global method involved representing $\phi(y)$ and is derivatives in terms of an expansion of Chebyshev polynomials. This is the method used by Bramley & Dennis (1982), and is based on a scheme of Orszag (1971) in his investigation of temporal stability of the Orr–Sommerfeld equation. The details of this numerical scheme can be found in Stocker (1992), but briefly, the solution is expressed in terms of (a finite number of) Chebyshev polynomials, and exploiting the orthogonal nature of these polynomials leads to a (linear) generalized eigenvalue problem of the form

$$(\boldsymbol{E}-\alpha\boldsymbol{F})\,\boldsymbol{\Phi}=0, \tag{9}$$

where

$$\boldsymbol{\Phi}=(\alpha^3\phi,\alpha^2\phi,\alpha\phi,\phi)^T, \tag{10}$$

which can be solved to find the eigenvalues α. The matrices $\boldsymbol{E}$ and $\boldsymbol{F}$ are $O((4N-12)\times(4N-12))$, where N is the number of Chebyshev polynomials considered, and ϕ consists of the set of Chebyshev coefficients. The NAG Library routine, F02BJF, was employed to solve (9), using the QZ algorithm of Moler & Stewart (1973). The advantages of this method are that it yields a whole range of eigenvalues and it does not require any initial data. The disadvantages are that computing time is $O(4^3[N+1]^3)$ and storage space is $O(4^2[N+1]^2)$, both of which become prohibitive for N large; also, some spurious eigenvalues are generated.

Our results were produced using a combination of these techniques. Finally, on account of the nature of (9), both α and its complex conjugate are eigenvalues; this will be implicitly assumed throughout the paper.

4. Plane Poiseuille flow: $\Psi_0'(y)=(y^2-1)$

For this case we set $V=0$ and $\gamma=-\frac{4}{3}$ in (5); this leads to the familiar quadratic velocity distribution, appropriate to flow through infinitely long straight channels with a constant streamwise pressure gradient. This particular problem has been studied in the past by Wilson (1969), and more recently by Bramley & Dennis (1982, 1984), and Bramley (1984). These latter papers were useful benchmarks for our numerical schemes. We undertook a thorough numerical investigation of this problem, starting at $R=0$, up to $R=4000$.

Before we continue, it must be noted that a differently scaled form of $\Psi_0'(y)$ was used in Wilson (1969) and Bramley & Dennis (1982), than has been used in this work. This not only results in the Reynolds number differing by a factor of 1.5, but it also implies that the upstream ($\mathrm{Re}(\alpha)<0$) eigenvalues found in Wilson (1969) and Bramley & Dennis (1982), correspond to our downstream ($\mathrm{Re}(\alpha)>0$) eigenvalues, and vice versa.

Our main check for the numerics in this case is with Bramley & Dennis (1982), which uses essentially the same global numerical scheme as in this work. For the complex eigenvalues in Bramley & Dennis (1982), the negative values agree exactly, and the positive values agree up to at least four decimal places, the discrepancy being due to the larger magnitude of the positive eigenvalues. The real eigenvalues also compare to at least four decimal places.

Although results have previously been presented for this problem, we believe these are not quite as comprehensive as some of our results described below. The symmetric nature of Poiseuille flow results in two distinct types of eigenfunctions – odd and even eigenfunctions about $y=0$.

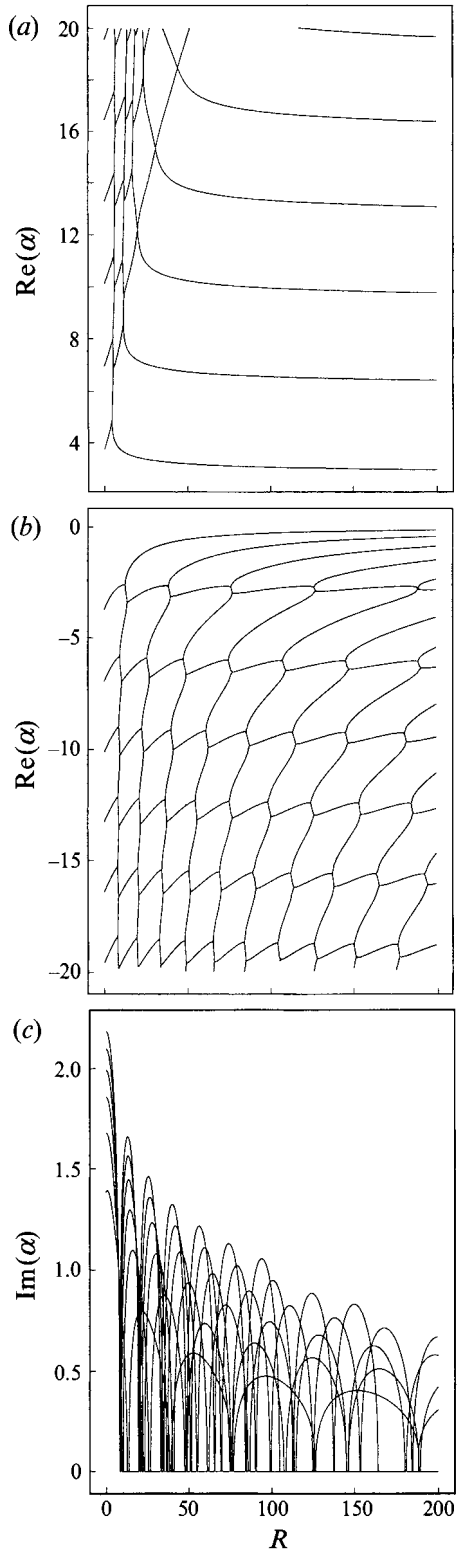

FIGURE 3. Odd eigenvalues for plane Poiseuille flow: (*a*) $\mathrm{Re}(\alpha) > 0$, (*b*) $\mathrm{Re}(\alpha) < 0$, (*c*) $\mathrm{Im}(\alpha)$.

4.1. $R \ll 1$ *modes*

At $R = 0$, all eigenvalues are complex. Following Wilson (1969), for $R \ll 1$, asymptotic expansions of the form

$$\phi = \tilde{\phi}_0 + R\tilde{\phi}_1 + \ldots \tag{11}$$

and

$$\alpha = \tilde{\alpha}_0 + R\tilde{\alpha}_1 + \ldots \tag{12}$$

can be used. The leading-order behaviour of the eigenvalues α is found by solving the equation

$$\sin 2\tilde{\alpha}_0 = \pm\tilde{\alpha}_0, \tag{13}$$

the positive sign giving $\tilde{\alpha}_0$ for the odd eigenvalues, and the negative sign for the even eigenvalues. Higher orders of approximation can be considered using standard techniques.

As R increases, branching of eigenvalues occurs, resulting in a 'honeycomb' pattern in (R, Re(α))-space, with the eigenvalues switching between complex conjugate pairs and real distinct values (or vice versa) at each branch point. These are shown in figures 3(*a*), 3(*b*) and 3(*c*) (figures 3*b* and 3*c* showing the real and complex parts respectively) for the odd eigenvalues, and in figures 4(*a*) and 4(*b*) for the even eigenvalues. A formula can be deduced to give the number of 'changes' from complex to real, or real to complex, before the eigenvalues take on their '$R \gg 1$' behaviour, i.e. before they become permanently real as R increases. This is applicable to all modes, except the first even mode for Re(α) < 0, which is a special case: the Pth mode has $2P$-1 changes (valid for $P \geqslant 1$).

We now move on to consider the eigenvalues in the limiting case of high-Reynolds-number flow.

4.2. $R \gg 1$, $\alpha = O(1)$ *modes*

First we look at the $O(1)$ real eigenvalue family found for Re(α) > 0. This family has been the subject of some disagreement, as the numerical work of Bramley & Dennis (1982) failed to identify the $O(1)$ family predicted by Wilson (1969) in his analytic work. Our numerical work resulted in an $O(1)$ family of eigenvalues with Re(α) > 0, whereas Wilson predicted eigenvalues with opposite sign (taking into account the different notation used). The analysis of these modes does closely follow that of Wilson (1969), and in fact is identical until the inner expansion about $y = -1$ is considered.

To recap, we take the solution to have the form

$$\phi = \phi_0 + \epsilon \ln \epsilon \phi_1 + \epsilon\phi_2 + \ldots \tag{14}$$

and

$$\alpha^2 = \alpha_0^2 + \epsilon \ln \epsilon \alpha_1^2 + \epsilon\alpha_2^2 + \ldots, \tag{15}$$

where $\epsilon = 1/(\alpha_0 R)^{1/3}$ is a small parameter. Substitution of these expansions into (7), leads to

$$\mathrm{D}_1 \phi_0 = 0 \tag{16}$$

and

$$\mathrm{D}_1 \phi_i = -\alpha_i^2 \phi_0 \quad \text{for} \quad i > 0, \tag{17}$$

where D_1 is the differential operator given by

$$\mathrm{D}_1 \equiv \frac{\mathrm{d}^2}{\mathrm{d}y^2} + \alpha_0^2 - \frac{2}{y^2 - 1}. \tag{18}$$

Equation (16) was solved numerically by utilizing the expansions (obtained by

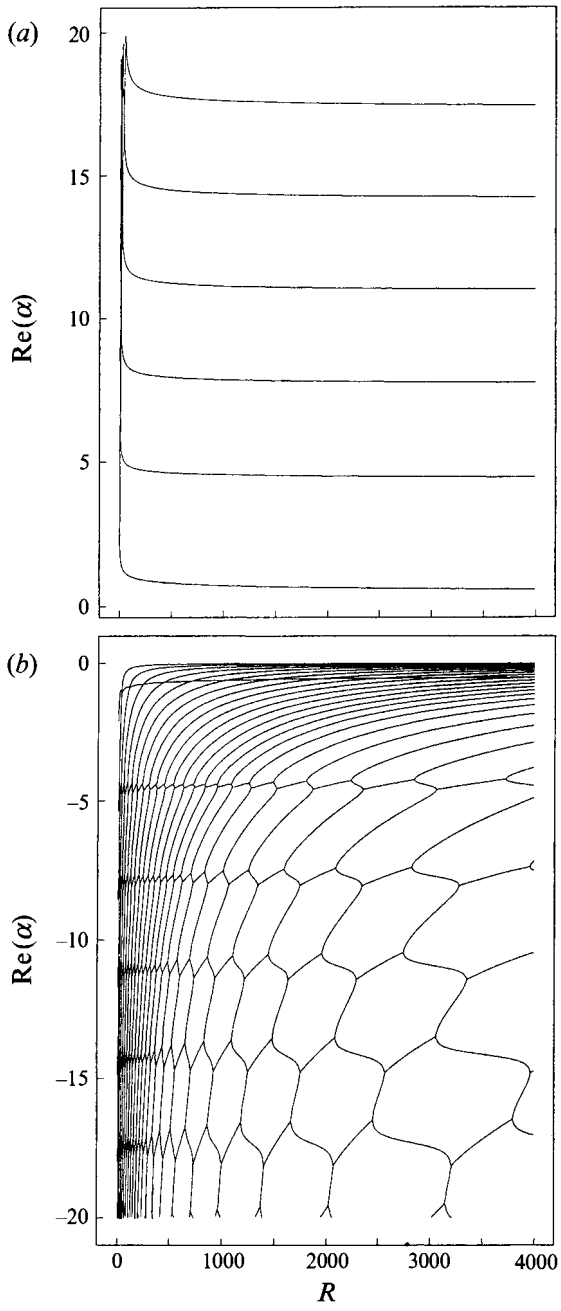

FIGURE 4. Even eigenvalues for plane Poiseuille flow: (*a*) $\mathrm{Re}(\alpha) > 0$, (*b*) $\mathrm{Re}(\alpha) < 0$.

applying the method of Frobenius, but see also Wilson 1969) about the point $y = -1$, namely

$$f_1(s) = s - \tfrac{1}{2}s^2 - \tfrac{1}{6}\alpha_0^2 s^3 + \ldots \tag{19}$$

and

$$f_2(s) = 1 + \ldots - f_1(s)\ln s, \tag{20}$$

where $s = y+1$, with $|s| \ll 1$. Considering the inner expansion close to $s = 0$ leads to the introduction of a stretched coordinate $\eta = (y+1)/\epsilon$, and the expansion

$$\phi \sim \epsilon(\hat{\phi}_0(\eta) + \epsilon \ln \epsilon \hat{\phi}_1(\eta) + \epsilon\hat{\phi}_2(\eta) + \ldots), \tag{21}$$

and it is found that

$$L_1 \hat{\phi}_0 = 0, \tag{22}$$

$$L_1 \hat{\phi}_1 = 0, \tag{23}$$

$$L_1 \hat{\phi}_2 = \left(2 - \eta^2 \frac{d^2}{d\eta^2}\right) \phi_0, \tag{24}$$

where $\hat{\phi}_i = \hat{\phi}_i(\eta)$ and

$$L_1 \equiv \frac{d^4}{d\eta^4} - 2\eta \frac{d^2}{d\eta^2}. \tag{25}$$

Solving (22) leads to

$$\hat{\phi}_0''(\hat{\eta}) = C_0 \operatorname{Ai}(\hat{\eta}) + D_0 \operatorname{Bi}(\hat{\eta}), \tag{26}$$

where C_0 and D_0 are constants, $\hat{\eta} = 2^{1/3}\eta$ and $\operatorname{Ai}(\hat{\eta})$ and $\operatorname{Bi}(\hat{\eta})$ are the two Airy functions. Rejection of $\operatorname{Bi}(\hat{\eta})$ (which is a non-physical solution to the problem), and integration of (26) leads to

$$\hat{\phi}_0(\hat{\eta}) = C_0 \int_0^{\hat{\eta}} \int_0^{\hat{\eta}_1} \operatorname{Ai}(\hat{\eta}_2)\, d\hat{\eta}_2\, d\hat{\eta}_1 + \hat{\eta} \frac{d\hat{\phi}_0}{d\hat{\eta}}(\hat{\eta} = 0) + \hat{\phi}_0(\hat{\eta} = 0). \tag{27}$$

Application of boundary conditions on $\eta = 0$, and consideration of the limit $\eta \to +\infty$ results in a form of the inner expansion which can be used to match onto the outer expansion. Including terms $O(\epsilon)$, the limiting form of the inner expansion is

$$\phi \sim a(\epsilon\eta - \tfrac{1}{2}\epsilon^2\eta^2) + b\epsilon(1 - \epsilon\eta \ln \eta), \tag{28}$$

where $a = \frac{1}{3}(2^{1/3})\, C_0$, $b = C_0 \operatorname{Ai}'(0)$ and for normalization purposes we set $C_0 = 3/2^{1/3}$. The outer expansion is of the form (see (19) and (20))

$$\begin{aligned}\phi = {} & (A_0 + \epsilon \ln \epsilon A_1 + \epsilon A_2 + \ldots)(s - \tfrac{1}{2}s^2 - \tfrac{1}{6}\alpha_0^2 s^3 + \ldots) \\ & + (B_0 + \epsilon \ln \epsilon B_1 + \epsilon B_2 + \ldots)(1 + \ldots - f_1(s) \ln s),\end{aligned} \tag{29}$$

where A_i and B_i are constants. Matching (28) and (29) yields boundary conditions for ϕ_0, ϕ_1 and ϕ_2 on $y = -1$.

In view of the symmetry of the problem, it is necessary to consider only half of the channel, say $-1 \leqslant y \leqslant 0$. So in order to solve (17) (to find α_1 and α_2), we require the boundary conditions for ϕ_0, ϕ_1 and ϕ_2 at $y = 0$. These were discussed by Wilson (1969), and are as follows:

$$\phi_0(-1) = 0, \quad \phi_0'(-1) = 1, \quad \begin{cases} \phi_0(0) = 0 & \text{for } \phi \text{ odd}, \\ \phi_0'(0) = 0 & \text{for } \phi \text{ even}, \end{cases} \tag{30, 31}$$

$$\phi_1(-1) = 0, \quad \begin{cases} \phi_1(0) = 0 & \text{for } \phi \text{ odd}, \\ \phi_1'(0) = 0 & \text{for } \phi \text{ even}, \end{cases} \tag{32, 33}$$

$$\phi_2(-1) = (3/2^{1/3}) \operatorname{Ai}'(0), \quad \begin{cases} \phi_2(0) = 0 & \text{for } \phi \text{ odd}, \\ \phi_2'(0) = 0 & \text{for } \phi \text{ even}. \end{cases} \tag{34, 35}$$

We are now in a position to solve (17), using adjoints. This leads to $\alpha_1 = 0$, and

$$\alpha_2^2 = \frac{\phi_2(-1)\, \phi^{\dagger'}(-1) - \phi_2(0)\, \phi^{\dagger'}(0)}{\int_{-1}^{0} \phi^\dagger \phi_0 \, dy} \quad \text{for } \phi \text{ odd}, \tag{36}$$

$$\alpha_2^2 = \frac{\phi_2(-1)\, \phi^{\dagger'}(-1) + \phi_2'(0)\, \phi^\dagger(0)}{\int_{-1}^{0} \phi^\dagger \phi_0 \, dy} \quad \text{for } \phi \text{ even}. \tag{37}$$

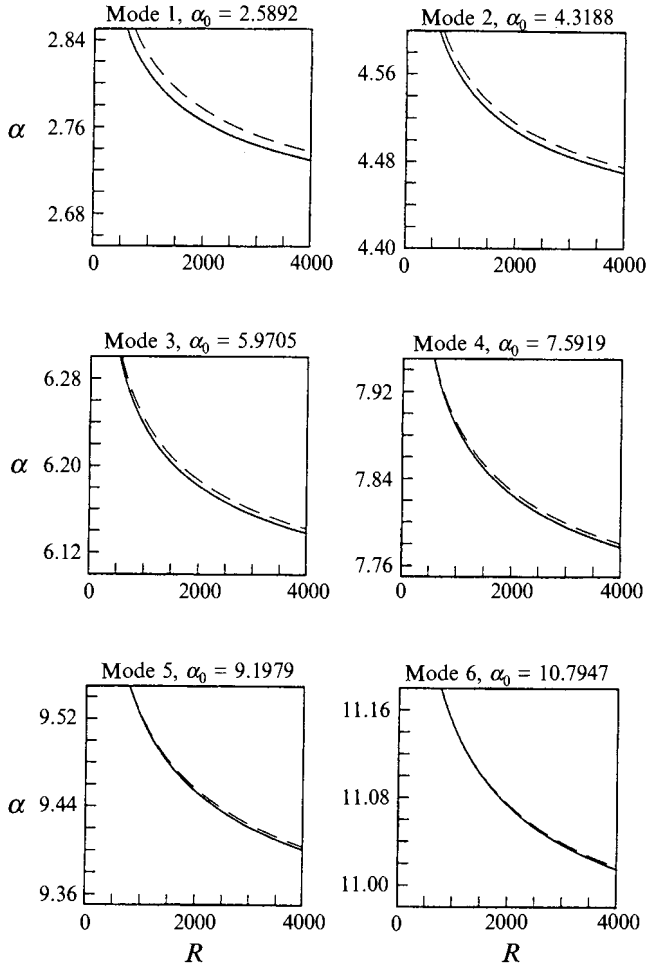

FIGURE 5. Eigenvalues for plane Poiseuille flow: comparison between numerical (——) and asymptotic (– – –) $R \gg 1$ results, for $\alpha = O(1)$ modes.

Eigenvalue	α_0	α_1	α_2
mode 1	2.5892	0.00	−3.2365
mode 2	4.3188	0.00	−4.0343
mode 3	5.9705	0.00	−4.9446
mode 4	7.5919	0.00	−5.8842
mode 5	9.1979	0.00	−6.8355
mode 6	10.7947	0.00	−7.7927

TABLE 1. Eigenvalues of Poiseuille flow

Note that since (16) is self-adjoint, $\phi^\dagger = \phi_0$. The numerical results for the first six modes are given in table 1.

Figure 5 shows the first three odd and first three even eigenvalues of this family with increase in Reynolds number. The dashed line is the asymptotic approximation for α given by

$$\alpha \sim \alpha_0 + \tfrac{1}{2}\alpha_2^2 \alpha_0^{-4/3} R^{-1/3} \quad \text{for} \quad \alpha_0 \neq 0, \tag{38}$$

Eigenvalue $\tilde{\tilde{\alpha}}_0$	$\Psi_0'(y) = (y^2-1)$	$\Psi_0'(y) = \frac{1}{4}(y+1)^2$	$\Psi_0'(y) = \frac{3}{4}(y+1)(y-\frac{1}{3})$	
			$\mathrm{Re}(\alpha) > 0$	$\mathrm{Re}(\alpha) < 0$
mode 1	−21.680	25.308	46.077	−169.45+19.68i
mode 2	−28.221	46.752	94.006	−549.86+43.83i
mode 3	−73.308	124.74	408.48	−1146.1+69.8i
mode 4	−86.284	174.74	580.04	−1958.2+96.9i
mode 5	−156.65	302.27	1216.5	
mode 6	−175.94	382.33	1526.5	

TABLE 2. $O(1/R)$ eigenvalues

and the solid line represents the value of the eigenvalue found by solving the full system (7). It appears that the asymptotic approximations improve for higher modes, the reason being that our analysis is based on the assumption that $|\epsilon| \ll 1$, and $|\epsilon|$ will be smaller for larger values of α_0.

The difficulty with Wilson's (1969) approach is that it is not possible to correctly match his wall-layer solution (close to $y = -1$) with the outer inviscid solution, if $\mathrm{Re}(\alpha) < 0$. This is not a problem, however, if $\mathrm{Re}(\alpha) > 0$.

4.3. $R \gg 1$, $\alpha = O(R^{-1/7})$ *modes*

Setting $\alpha_0 = 0$ in (15) results in two eigenvalues developing in the form

$$\alpha \sim \tfrac{1}{2}[-90\mathrm{Ai}'(0)]^{3/7}R^{-1/7}, \quad \alpha \sim \tfrac{1}{2}e^{6i\pi/7}[-90\mathrm{Ai}'(0)]^{3/7}R^{-1/7}. \tag{39a, b}$$

Equation 39(a) corresponds to the 'upstream' eigensolution as found by Smith (1977), and is a positive real even mode. Equation (39b) is an even mode, which remains complex for all Reynolds numbers, and has $\mathrm{Re}(\alpha) < 0$. It can be seen in figure 4(b) and was also found in other studies (Wilson 1969 and Bramley & Dennis 1982) (see the Appendix).

4.4. $R \gg 1$, $\alpha = O(1/R)$ *modes*

The other downstream eigenvalue families for $R \gg 1$ all turn out to have $\alpha = O(1/R)$, and following Wilson (1969), their expansions take the form

$$\phi = \phi_0 + \frac{1}{R}\phi_1 + \frac{1}{R^2}\phi_2 \ldots \tag{40}$$

and

$$\alpha = \frac{1}{R}\tilde{\tilde{\alpha}}_0 + \frac{1}{R^2}\tilde{\tilde{\alpha}}_1 + \frac{1}{R^3}\tilde{\tilde{\alpha}}_2 \ldots. \tag{41}$$

Neglecting terms of $O(1/R)$ in (7) we obtain the equation

$$\phi_0^{\mathrm{iv}} + \tilde{\tilde{\alpha}}_0(y^2-1)\phi_0'' - 2\tilde{\tilde{\alpha}}_0\phi_0 = 0, \tag{42}$$

which can be solved numerically (in much the same way as (7)), applying the impermeability and no-slip boundary conditions, to give $\tilde{\tilde{\alpha}}_0$. Table 2 shows the results thus obtained. The asymptotic and numerical results are graphically indistinguishable for $R \gg 1$, and are therefore not presented graphically. These eigenvalues also agree with the results of Wilson (1969), when the differing form of $\Psi_0(y)$ is taken into

account. Physically, we are interested in the eigenvalue whose real part is smallest in magnitude, as this will be the eigenvalue which corresponds to the mode that persists further (decays slowest) downstream. This is the eigenvalue of the form

$$\alpha \sim -21.68/R + O(1/R^2). \tag{43}$$

In summary, as $R \to \infty$, for $\mathrm{Re}(\alpha) > 0$ there exists one real $O(1)$ eigenvalue family, and one real eigenvalue $O(R^{-1/7})$; for $\mathrm{Re}(\alpha) < 0$ there exists one real $O(1/R)$ eigenvalue family, together with one complex eigenvalue $O(R^{-1/7})$.

In the following section we go on to consider a particular combination of γ and V that almost leads to flow reversal at $y = -1$.

5. The intermediate case: $\Psi_0'(y) = \frac{1}{4}(y+1)^2$

If $V = 1$ and $\gamma = \frac{2}{3}$ then the velocity profile above is obtained. The interesting feature of this basic flow is that $\Psi_0''(-1) = \Psi_0'(-1) = 0$, and so it is a marginal case, on the verge of reversing on the lower wall. The eigenvalues obtained by solving the full system (7) are shown in figure 6(*a*) ($\mathrm{Re}(\alpha) > 0$; the imaginary part of α is not shown in the interest of brevity) and 6(*b*) ($\mathrm{Re}(\alpha) < 0$; note that this is a real family of eigensolutions). As in the previous case, branching of eigenvalues occurs for R small. At $R = 0$, the complex eigenvalues found from the solution of (13) are valid for any $\Psi_0'(y)$, and thus are valid here. For $R \gg 1$, it appears that we once again obtain an $O(1/R)$ real eigenvalue family for $\mathrm{Re}(\alpha) > 0$ and an $O(1)$ real eigenvalue family for $\mathrm{Re}(\alpha) < 0$.

5.1. $R \gg 1$, $\alpha = O(1/R)$ *modes*

Starting with the downstream ($\mathrm{Re}(\alpha) > 0$) eigenvalues, our numerical investigation leads us to seek, asymptotically, an $O(1/R)$ eigenvalue family as $R \to \infty$. Expansions (40) and (41) are again substituted into (7) resulting in the leading-order equation

$$\phi_0^{\mathrm{iv}} + \tilde{\tilde{\alpha}}_0 \tfrac{1}{4}(y+1)^2 \phi_0'' - \tfrac{1}{2}\tilde{\tilde{\alpha}}_0 \phi_0 = 0, \tag{44}$$

which can be solved in much the same manner as (7) and (42), to give $\tilde{\tilde{\alpha}}_0$. Table 2 shows the results thus obtained. Once again the asymptotic and numerical results are graphically indistinguishable for $R \gg 1$.

5.3. $R \gg 1$, $\alpha = O(1)$ *modes*

For $\mathrm{Re}(\alpha) < 0$, we now seek an $O(1)$ real eigenvalue family as $R \to \infty$, and proceed in a similar manner to the previous case. The nature of these eigenvalues is altered, however, because in this case not only $\Psi_0'(-1) = 0$, but also $\Psi_0''(-1) = 0$. The solution in the core region turns out to develop in the form

$$\phi = \phi_0 + \delta\phi_1 + \delta^2\phi_2 + \ldots \tag{45}$$

and

$$\alpha^2 = \alpha_0^2 + \delta\alpha_1^2 + \delta^2\alpha_2^2 + \ldots, \tag{46}$$

where $\delta = 1/(-\alpha_0 R)^{1/4}$ is a small parameter. Substitution of these expansions into (7) results in

$$\mathrm{D}_2 \phi_0 = 0, \tag{47}$$

and

$$\mathrm{D}_2 \phi_i = -\alpha_i^2 \phi_0 \quad \text{for} \quad i > 0, \tag{48}$$

where D_2 is the differential operator

$$\mathrm{D}_2 \equiv \frac{\mathrm{d}^2}{\mathrm{d}y^2} + \alpha_0^2 - \frac{2}{(y+1)^2}. \tag{49}$$

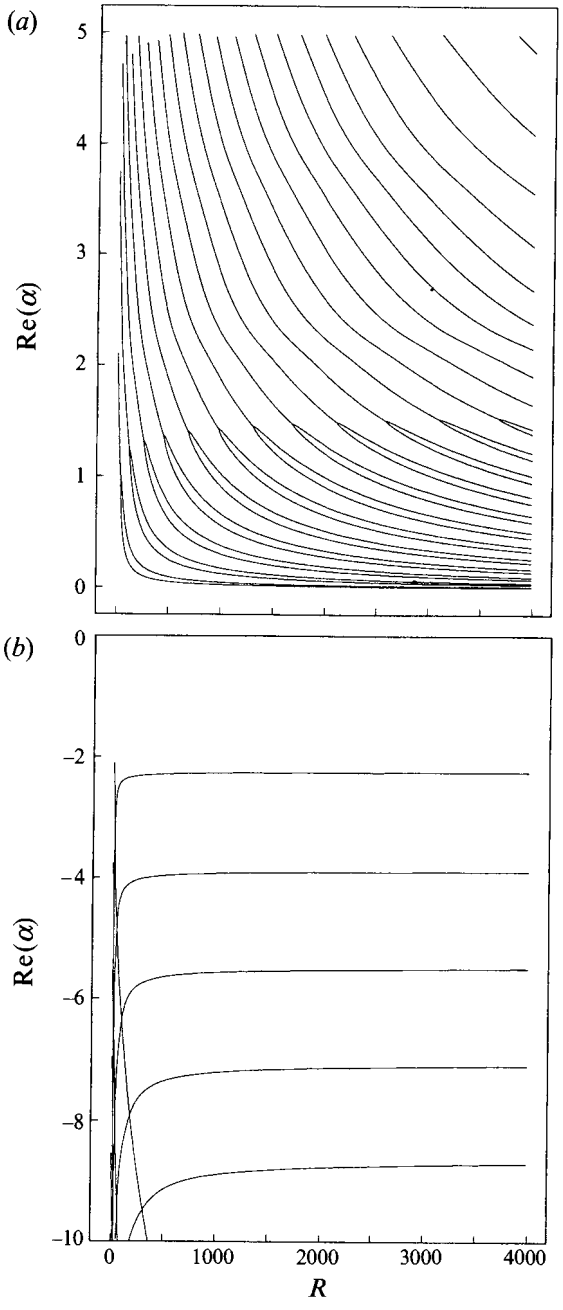

FIGURE 6. Eigenvalues for the intermediate case: (*a*) $\mathrm{Re}(\alpha) > 0$, (*b*) $\mathrm{Re}(\alpha) < 0$.

The method of Frobenius yields the following behaviour for the two linearly independent solutions as $s \to 0$:

$$g_1(s) = s^2 - \frac{\alpha_0^2}{10}s^4 + \frac{\alpha_0^4}{280}s^6 + \ldots \tag{50}$$

and

$$g_2(s) = \frac{1}{s} + \frac{\alpha_0^2 s}{2} - \frac{\alpha_0^4 s^3}{8} + \ldots, \tag{51}$$

where again $s = y+1$. Considering the inner expansion close to $s = 0$ leads to the introduction of the stretched coordinate $\zeta = (y+1)/\delta$. The inner expansion in this region develops in the form

$$\phi \sim \delta^2(\hat{\phi}_0(\zeta)+\delta\hat{\phi}_1(\zeta)+\delta^2\hat{\phi}_2(\zeta)+\ldots), \tag{52}$$

where
$$\mathrm{L}_2\hat{\phi}_0 = 0, \tag{53}$$
$$\mathrm{L}_2\hat{\phi}_1 = 0, \tag{54}$$
and
$$\mathrm{L}_2\hat{\phi}_2 = \alpha_0^2[\tfrac{1}{4}\zeta^2 - 2\,\mathrm{d}^2/\mathrm{d}\zeta^2]\phi_0, \tag{55}$$
with
$$\mathrm{L}_2 \equiv \mathrm{d}^4/\mathrm{d}\zeta^4 - \tfrac{1}{4}\zeta^2\,\mathrm{d}^2/\mathrm{d}\zeta^2 + \tfrac{1}{2}. \tag{56}$$

One exact solution of (53) is $\hat{\phi}_0 = A\zeta^2$, where A is a constant. The general solution which is valid in the limit as $\zeta \to +\infty$ is

$$\hat{\phi}_0(\zeta) \sim A\zeta^2 + B/\zeta + C\exp(-\tfrac{1}{4}\zeta^2) + D\exp(\tfrac{1}{4}\zeta^2), \tag{57}$$

where A, B, C and D are constants. For a physically realistic solution, we require $D = 0$. The limit of the inner expansion as $\zeta \to \infty$ is then

$$\phi(\zeta) \sim A\delta^2(\zeta^2 + O(\delta^2)) + B\delta^2(1/\zeta + O(\delta^2)). \tag{58}$$

Recasting this in terms of s leads to

$$\phi \sim (A+O(\delta^2))\left(s^2 - \frac{\alpha_0^2}{10}s^4 + \ldots\right) + (B\delta^3 + O(\delta^4))\left(\frac{1}{s} + \frac{\alpha_0^2 s}{2} - \frac{\alpha_0^4 s^3}{8} + \ldots\right). \tag{59}$$

This must be matched with the outer expansion as $s \to 0$ which is taken to be of the form

$$\phi = (A_0 + \delta A_1 + \delta^2 A_2 + \delta^3 A_3 + \delta^4 A_4 + \ldots)\left(s^2 - \frac{\alpha_0^2}{10}s^4 + \frac{\alpha_0^4}{280}s^6 + \ldots\right)$$
$$+ (B_0 + \delta B_1 + \delta^2 B_2 + \delta^3 B_3 + \delta^4 B_4 + \ldots)\left(\frac{1}{s} + \frac{\alpha_0^2 s}{2} - \frac{\alpha_0^4 s^3}{8} + \ldots\right), \tag{60}$$

where A_i and B_i are constants.

In order to solve (47) we must also investigate the upper wall layer on $y = +1$. Writing

$$\phi = \delta^2\Phi(Y) + \ldots, \tag{61}$$

where $\Phi(Y)$ is $O(1)$, leads to a general solution of the form

$$\Phi(Y) = -K_0\frac{Y}{-\alpha^{3/2}} - K_3 + \frac{K_1}{-\alpha^{1/2}}\mathrm{e}^{-Y} + \frac{K_2}{-\alpha^{1/2}}\mathrm{e}^{+Y}, \tag{62}$$

where K_0, K_2, K_3 are constants, and $Y = (y-1)/\delta^2$. Application of the no-slip and impermeability boundary conditions on $y = +1$, and consideration of only physically realistic solutions to the problem gives

$$\phi(y) = -K_3[1 + Y - \mathrm{e}^{+Y}]. \tag{63}$$

Normalizing by setting $K_3 = -1$ leads to the requirement that, as $y \to 1$,

$$\phi(y) = (y-1) + \delta^2 + \text{e.s.t.} \tag{64}$$

where e.s.t. stands for exponentially small terms. Therefore (also taking into account (59) and (60)) the relevant boundary conditions for the core solution terms ϕ_i are as follows:

$$\phi_0(-1) = 0, \quad \phi_0(1) = 0, \tag{65}$$
$$\phi_0'(-1) = 0, \quad \phi_0'(1) = 1, \tag{66}$$
$$\phi_1(-1) = 0, \quad \phi_1(1) = 0, \tag{67}$$
$$\phi_2(-1) = 0, \quad \phi_2(1) = 1. \tag{68}$$

Eigenvalue	α_0	α_1	α_2
mode 1	−2.2467	0.00	1.1234
mode 2	−3.8626	0.00	1.9313
mode 3	−5.4521	0.00	2.7260
mode 4	−7.0331	0.00	3.5165
mode 5	−8.6104	0.00	4.3052
mode 6	−10.1857	0.00	5.0928

TABLE 3. Eigenvalues for the intermediate case

As with the previous case, (48) can be solved using adjoints. This results in $\alpha_1 = 0$, and

$$\alpha_2^2 = \frac{-\phi_2(1)\,\phi^{\dagger\prime}(1) + \phi_2'(1)\,\phi^{\dagger}(1)}{\int_{-1}^{1} \phi^{\dagger}\phi_0\,\mathrm{d}y}, \tag{69}$$

where, again $\phi^{\dagger} = \phi_0$.

The numerical details are given in table 3, obtained using a Runge–Kutta scheme. Figure 7 compares the numerical and asymptotic results. The dashed line gives the asymptotic approximation given by

$$\alpha \sim \alpha_0 + \tfrac{1}{2}\alpha_2^2(-\alpha_0)^{-5/2}R^{-1/2} \quad \text{for} \quad \alpha_0 \neq 0, \tag{70}$$

and the solid line is the value of the eigenvalue found by solving (7). The agreement is not unsatisfactory, in particular the lower modes give good agreement, and the numerical and asymptotic values are seen to converge as R increases.

6. The driven-cavity case: $\Psi_0'(y) = \frac{3}{4}(y+1)(y-\frac{1}{3})$

In the case of a basic flow driven solely by the sliding top ($V = 1$), with no imposed streamwise pressure gradient and with no net mass flux ($\gamma = 0$), the fully developed velocity profile must take on the above form. The flow cannot be unidirectional, and indeed reverses (relative to the upper boundary motion) for $y \in [-1, \frac{1}{3}]$. Figures 8(*a*) and 8(*b*) show the $\mathrm{Re}(\alpha) > 0$ and $\mathrm{Re}(\alpha) < 0$ (respectively) eigenvalue families for this case obtained by solving (7) numerically. Some branching at low Reynolds numbers occurs as with the previous two cases, but not in a nearly so regular fashion. All the eigenvalues originate in a complex form (from the solution of (13), as before) and develop into four distinct eigenvalue families for $R \gg 1$.

Consider first the downstream eigenvalues, i.e. those with $\mathrm{Re}(\alpha) > 0$. These turn out to consist of two real eigenvalue families – an $O(1)$ and an $O(1/R)$ family.

6.1. $R \gg 1$, $\alpha = O(1)$, $Re(\alpha) > 0$ *modes*

The $O(1)$ family is of much interest, partly because the eigenvalues turn out to leading order to be a scaled form of the $O(1)$ Poiseuille flow eigenvalues. This can be explained by taking expansions for ϕ and α of the form

$$\phi = \phi_0 + \cos((\alpha_0 R)^{1/2} I + \tfrac{1}{4}\pi)\,\epsilon^{3/4}\phi_1 + \epsilon \ln \epsilon \phi_2 + \epsilon\phi_3 + \ldots, \tag{71}$$

and

$$\alpha^2 = \alpha_0^2 + \cos((\alpha_0 R)^{1/2} I + \tfrac{1}{4}\pi)\,\epsilon^{3/4}\alpha_1^2 + \epsilon \ln \epsilon \alpha_2^2 + \epsilon\alpha_3^2 + \ldots, \tag{72}$$

where $\epsilon = 1/(\alpha_0 R)^{1/3}$ is a small parameter, and

$$I = \tfrac{2}{3}(1 - (1/\sqrt{3})\sinh^{-1}(1/\sqrt{2})). \tag{73}$$

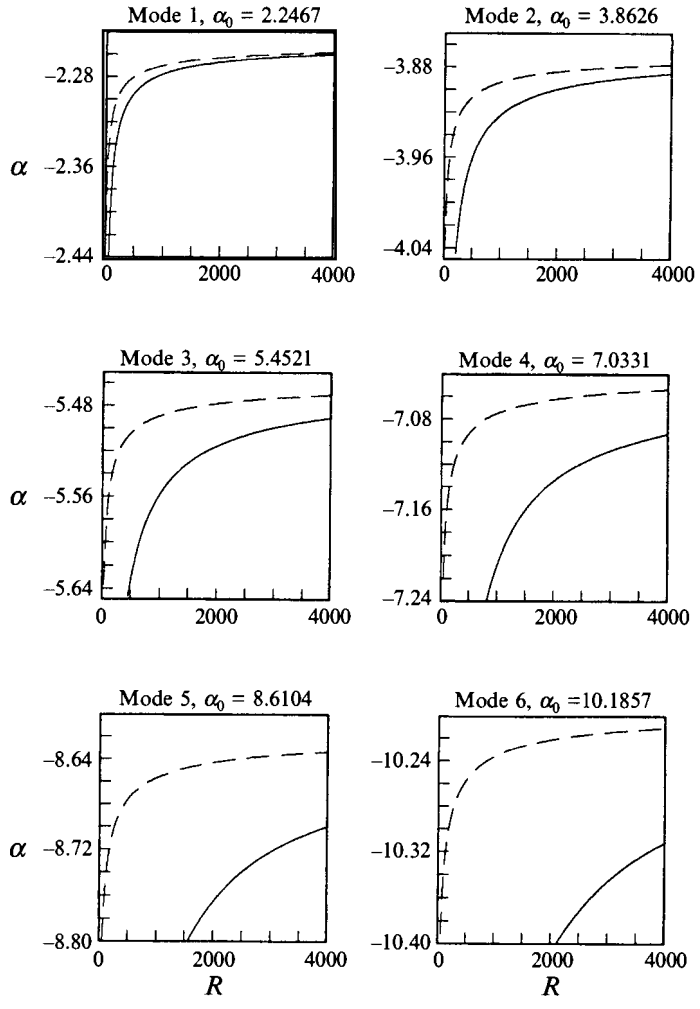

FIGURE 7. Eigenvalues for the intermediate case: comparison between numerical (——) and asymptotic (– – –) $R \gg 1$ results, for $\alpha = O(1)$ modes.

The cosine terms (involving the square root of the Reynolds number) appear quite novel, and are unexpected, but the ensuing analysis and our numerical results both conclusively indicate their presence. Substitution of (71) and (72) into (7), and letting $R \to \infty$ results in the equations

$$\mathrm{D}_3 \phi_0 = 0, \tag{74}$$

and

$$\mathrm{D}_3 \phi_i = -\alpha_i^2 \phi_0 \quad \text{for} \quad i > 0, \tag{75}$$

where D_3 is the differential operator given by

$$\mathrm{D}_3 \equiv \frac{\mathrm{d}^2}{\mathrm{d}y^2} + \alpha_0^2 - \frac{2}{(y+1)(y-\frac{1}{3})}. \tag{76}$$

By considering the transformation

$$y = \tfrac{1}{3}(2\hat{y} - 1), \tag{77}$$

we can obtain (16) from (74) (with $\hat{y}$ replacing y). Next consider the boundary

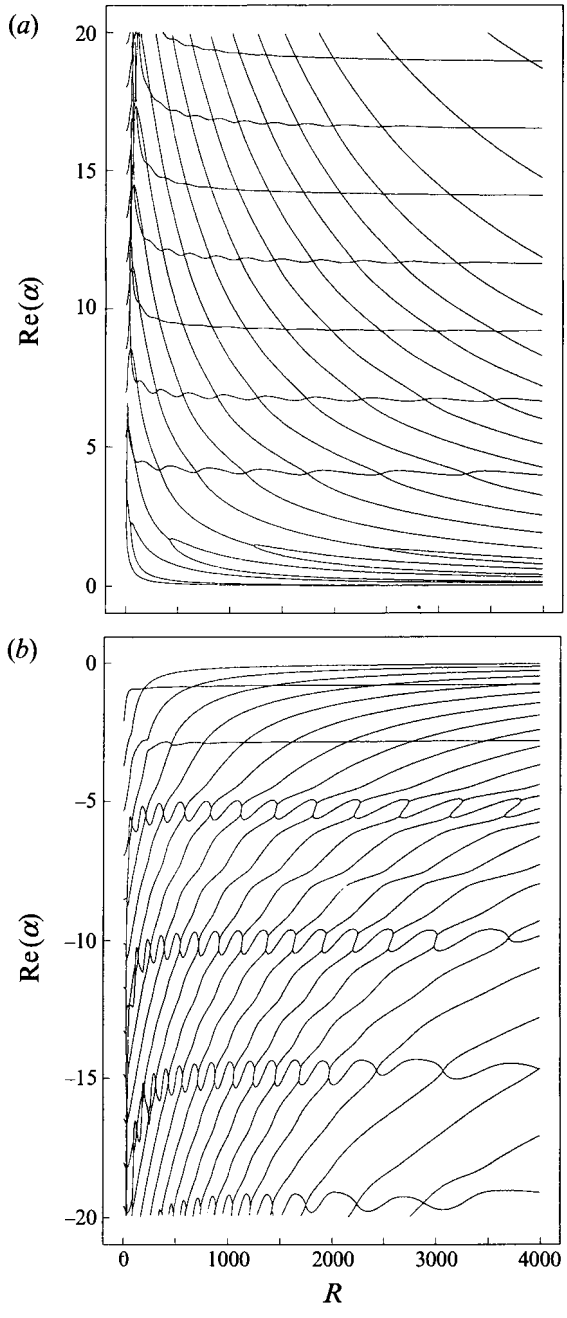

FIGURE 8. Eigenvalues for the long driven-cavity case: (*a*) $\mathrm{Re}(\alpha) > 0$, (*b*) $\mathrm{Re}(\alpha) < 0$.

conditions for ϕ_0; in the case of Poiseuille flow (as considered in §4), the appropriate boundary conditions were $\phi_0(-1) = \phi_0(1) = 0$. In the present case, we again have $\phi_0(-1) = 0$ due to the impermeability condition on the lower wall. Consideration of the singularities and critical layer (see (88)–(97) below) leads us to conclude that $\phi_0(\frac{1}{3}) = 0$, and results in a simple relationship between the leading-order terms of the driven-cavity case (dc), and the Poiseuille flow case (pf), namely

$$\alpha_0^{dc} = \tfrac{3}{2}\alpha_0^{pf}. \tag{78}$$

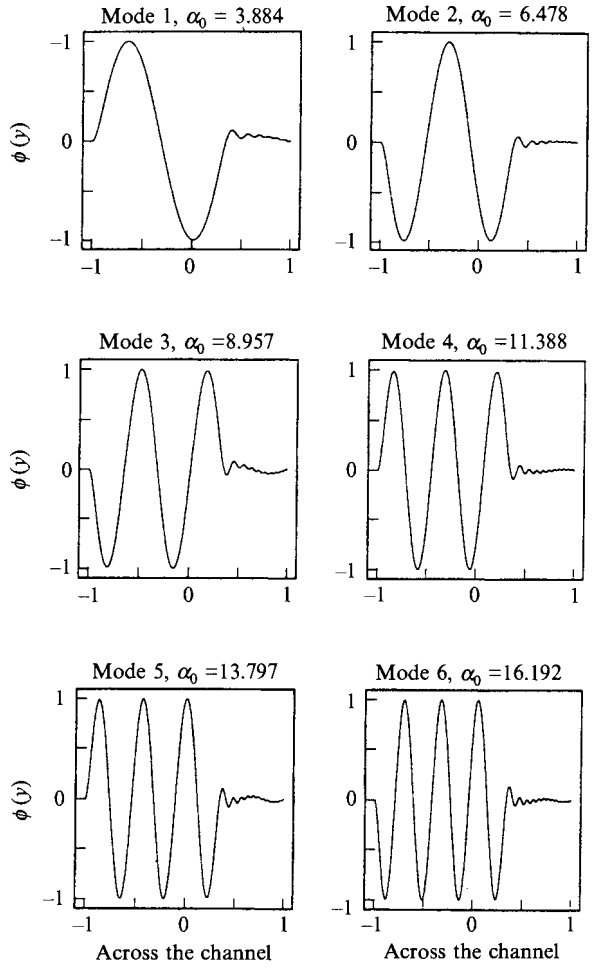

FIGURE 9. Eigenfunctions for the long driven-cavity case, $R = 2000$.

Figure 9 shows eigenfunctions for these $O(1)$ real positive eigenvalues obtained numerically by solving (7) with the appropriate base flow, at $R = 2000$. These confirm that the eigenfunctions are, to a large extent, confined to the region $y \in [-1, \frac{1}{3}]$ in accord with the arguments above, leading to (78).

For later reference, the two linearly independent solutions of (74) about $y = -1$ take the form

$$h_1(s) = s - \tfrac{3}{4}s^2 - \frac{\alpha_0^2}{6}s^3 + \frac{\alpha_0^2}{12}s^4 + \ldots, \tag{79}$$

and

$$h_2(s) = 1 - \ldots - \tfrac{3}{2}h_1(s)\ln s, \tag{80}$$

where $s = y + 1$, whilst about $y = \frac{1}{3}$ the linearly independent solutions take the form

$$r_1(t) = K\left(t + \frac{3}{4}t^2 - \frac{\alpha_0^2}{6}t^3 + \frac{\alpha_0^2}{12}t^4 + \ldots\right), \tag{81}$$

and

$$r_2(t) = 1 - \ldots + (3/2K)f_1(t)\ln t, \tag{82}$$

where $t = y - \frac{1}{3}$, and $K = \pm 1$ (as a result of the normalization process and symmetry/antisymmetry).

The region $y \in [\frac{1}{3}, 1]$ is considered next. Though it is tempting to consider equations of the form (74) in this region, this leads to inconsistencies, and it turns out instead that in this region a WKB approximation is appropriate. Taking α to be $O(1)$, and retaining only the highest-order terms of each derivative, we obtain the equation

$$(\mathrm{d}^4/\mathrm{d}y^4 + \alpha R \Psi_0'(y)\,\mathrm{d}^2/\mathrm{d}y^2 - \tfrac{3}{2}\alpha R)\,\phi = 0. \tag{83}$$

Looking for *highly oscillatory* solutions to this problem, the assumption $\mathrm{d}/\mathrm{d}y \gg 1$ implies

$$(\mathrm{d}^4/\mathrm{d}y^4 + \alpha R \Psi_0'(y)\,\mathrm{d}^2/\mathrm{d}y^2)\,\phi \approx 0, \tag{84}$$

and the first-order WKB approximation to ϕ_0 in this region is

$$\phi(y) = -\frac{A}{\alpha R(\Psi_0'(y))^{5/4}} \exp\left[\mathrm{i}(\alpha R)^{1/2} \int_{y_0}^{y} (\Psi_0'(\tilde{y}))^{1/2}\,\mathrm{d}\tilde{y}\right]$$
$$-\frac{B}{\alpha R(\Psi_0'(y))^{5/4}} \exp\left[-\mathrm{i}(\alpha R)^{1/2} \int_{y_0}^{y} (\Psi_0'(\tilde{y}))^{1/2}\,\mathrm{d}\tilde{y}\right] + \gamma_1 y + \gamma_2. \tag{85}$$

Here γ_1 and γ_2 are constants, and $y_0 = \frac{1}{3}$. The boundary conditions at $y = +1$ (no-slip and impermeability) require $\phi(1) = \phi'(1) = 0$, which leads to

$$-(1/\alpha R)\,[A \exp(\mathrm{i}(\alpha R)^{1/2} I) + B \exp(-\mathrm{i}(\alpha R)^{1/2} I)] + \gamma_1 + \gamma_2 = 0, \tag{86}$$

and

$$-(1/\alpha R)^{1/2}\,[A \exp(\mathrm{i}(\alpha R)^{1/2} I) - B \exp(-\mathrm{i}(\alpha R)^{1/2} I)] + \gamma_1 = 0. \tag{87}$$

Equations (86) and (87) serve to determine γ_1 and γ_2 in terms of A and B.

In order to find a relationship between A and B, we must look in more detail at the critical layer at $y = \frac{1}{3}$ (this also confirms our boundary condition for $\phi_0(\frac{1}{3})$). Using the scaled coordinate $\eta = (y - \frac{1}{3})/\epsilon$, and the expansion

$$\phi \sim \cos((\alpha R)^{1/2} I + \tfrac{1}{4}\pi)\,\epsilon^{3/4} \hat{\phi}_0(\eta) + \epsilon \ln \epsilon \hat{\phi}_1(\eta) + \epsilon \hat{\phi}_2(\eta) + \ldots, \tag{88}$$

we obtain

$$\mathrm{L}_3 \hat{\phi}_i = 0 \quad \text{for} \quad i = 0, 1, 2, \tag{89}$$

where $\hat{\phi}_i = \hat{\phi}_i(\eta)$ and

$$\mathrm{L}_3 \equiv \mathrm{d}^4/\mathrm{d}\eta^4 + \eta\,\mathrm{d}^2/\mathrm{d}\eta^2. \tag{90}$$

The general solution to (89) may be written

$$\hat{\phi}_i''(\eta) = C_i \mathrm{Ai}(-\eta) + D_i \mathrm{Bi}(-\eta) \quad \text{for} \quad i = 0, 1, 2, \tag{91}$$

where C_i and D_i are constants. Rejecting $\mathrm{Bi}(-\eta)$ as an unbounded solution to the problem, leads to

$$\hat{\phi}_i(\eta) = C_i \int_0^{\eta} \int_0^{\eta_1} \mathrm{Ai}(-\eta_2)\,\mathrm{d}\eta_2\,\mathrm{d}\eta_1 + \eta \frac{\mathrm{d}\hat{\phi}_i}{\mathrm{d}\eta}(\eta = 0) + \hat{\phi}_i(\eta = 0). \tag{92}$$

In the limit $\eta \to +\infty$

$$\hat{\phi}_i \sim \left[\tfrac{2}{3} C_i + \frac{\mathrm{d}\hat{\phi}_i}{\mathrm{d}\eta}(\eta = 0)\right]\eta + C_i \mathrm{Ai}'(0) + \hat{\phi}_i(\eta = 0) - \frac{7}{48\pi^{1/2}} C_i \eta^{-5/4} \sin(\tfrac{2}{3}\eta^{3/2} + \tfrac{1}{4}\pi), \tag{93}$$

whilst as $\eta \to -\infty$

$$\hat{\phi}_i \sim \left[-\tfrac{1}{3} C_i + \frac{\mathrm{d}\hat{\phi}_i}{\mathrm{d}\eta}(\eta = 0)\right]\eta + C_i \mathrm{Ai}'(0) + \hat{\phi}_i(\eta = 0). \tag{94}$$

The oscillatory terms in the limit as $\eta \to +\infty$ match with the oscillatory (exponential) terms in the WKB expansion to give a relationship between the complex coefficients A and B, and together with (86) and (87) leads to the following form for the solution in the region $y \in [\frac{1}{3}, 1]$:

$$\phi(y) \sim Q\left[\frac{\epsilon^{3/2}}{(\Psi_0'(y))^{5/4}} \sin((\alpha R)^{1/2} g(y) + \tfrac{1}{4}\pi) + (1-y)\cos((\alpha R)^{1/2} I + \tfrac{1}{4}\pi) - \epsilon^{3/2} \sin((\alpha R)^{1/2} I + \tfrac{1}{4}\pi)\right], \quad (95)$$

where

$$Q = h(\epsilon)\left[-\frac{7}{48\pi^{1/2}} C_2 \epsilon^{-1/4}\right], \quad (96)$$

$$g(y) = (2/3\sqrt{3})\{\tfrac{3}{8}(y-\tfrac{1}{3})^{1/2}(y+1)^{1/2}(3y+1) - \sinh^{-1}[\tfrac{1}{2}\sqrt{3}(y-\tfrac{1}{3})^{\frac{1}{2}}]\}, \quad (97)$$

$A = \frac{1}{2}Q\mathrm{i}(\alpha R)^{1/2}$, $B = -\frac{1}{2}Q\mathrm{i}(\alpha R)^{1/2}$, and $h(\epsilon)$ is a scaling which will be determined shortly.

The outer expansion for ϕ (from (81)) gives

$$\phi_0 \sim K(y - \tfrac{1}{3}) \quad \text{as} \quad y \to \tfrac{1}{3}(y < \tfrac{1}{3}). \quad (98)$$

This must match with $\hat{\phi}_2$ as $\eta \to -\infty$, and so from (94),

$$-\tfrac{1}{3}C_2 + (\mathrm{d}\hat{\phi}_2/\mathrm{d}\eta)(\eta = 0) = K. \quad (99)$$

This implies $h(\epsilon) = \epsilon$ and then the linear (and largest) term in the WKB expansion is $O(\epsilon^{3/4})$. As there is no $O(\epsilon)$ term in the region $y \in [\frac{1}{3}, 1]$,

$$\tfrac{2}{3}C_2 + (\mathrm{d}\hat{\phi}_2/\mathrm{d}\eta)(\eta = 0) = 0, \quad (100)$$

and

$$C_2 \mathrm{Ai}'(0) + \hat{\phi}_2(\eta = 0) = 0. \quad (101)$$

Equations (99) and (100) give $C_2 = -K$, and (101) gives us the boundary condition for ϕ_3:

$$\phi_3(y = \tfrac{1}{3}) = 0. \quad (102)$$

We now know that the ϕ-expansion in $y \in [\frac{1}{3}, 1]$ is, to leading order, of the form

$$\phi \sim \frac{7}{48\pi^{1/2}} K(1-y)\cos((\alpha R)^{1/2} I + \tfrac{1}{4}\pi)\,\epsilon^{3/4}. \quad (103)$$

This outer expansion for ϕ is consistent with the inner expansions (93) and (94) provided $C_0 = 0$ and $\hat{\phi}_0(\eta) \equiv (7/72\pi^{1/2})K$. The boundary condition for ϕ_1 arises from (103) evaluated at $y = \frac{1}{3}$, i.e.

$$\phi_1(y = \tfrac{1}{3}) = (7/72\pi^{1/2})K. \quad (104)$$

Finally, in the singular layer, there are no $O(\epsilon \ln \epsilon)$ terms, so $\hat{\phi}_1 = 0$ and $\phi_2(y = \frac{1}{3}) = 0$.

Next consider the boundary layer on $y = -1$. This layer has the same structure as the layers on $y = \pm 1$ for the Poiseuille flow case. The expansions (79) and (80) give the outer solution in this region. The inner expansion in this region takes the form

$$\phi \sim \epsilon(\Phi_0(\zeta) + \cos((\alpha R)^{1/2} I + \tfrac{1}{4}\pi)\,\epsilon^{3/4}\Phi_1(\zeta) + \epsilon \ln \epsilon \Phi_2(\zeta) + \epsilon\Phi_3(\zeta)\ldots), \quad (105)$$

where $\zeta = (y+1)/\epsilon$. Equating powers of ϵ, we obtain

$$\mathrm{H}\Phi_0 = 0 \quad (106)$$

where $\Phi_0 = \Phi_0(\zeta)$ and

$$\mathrm{H} \equiv \mathrm{d}^4/\mathrm{d}\zeta^4 - \zeta\,\mathrm{d}^2/\mathrm{d}\zeta^2. \quad (107)$$

This gives

$$\Phi_0'' = A_1 \mathrm{Ai}(\zeta) + A_2 \mathrm{Bi}(\zeta). \quad (108)$$

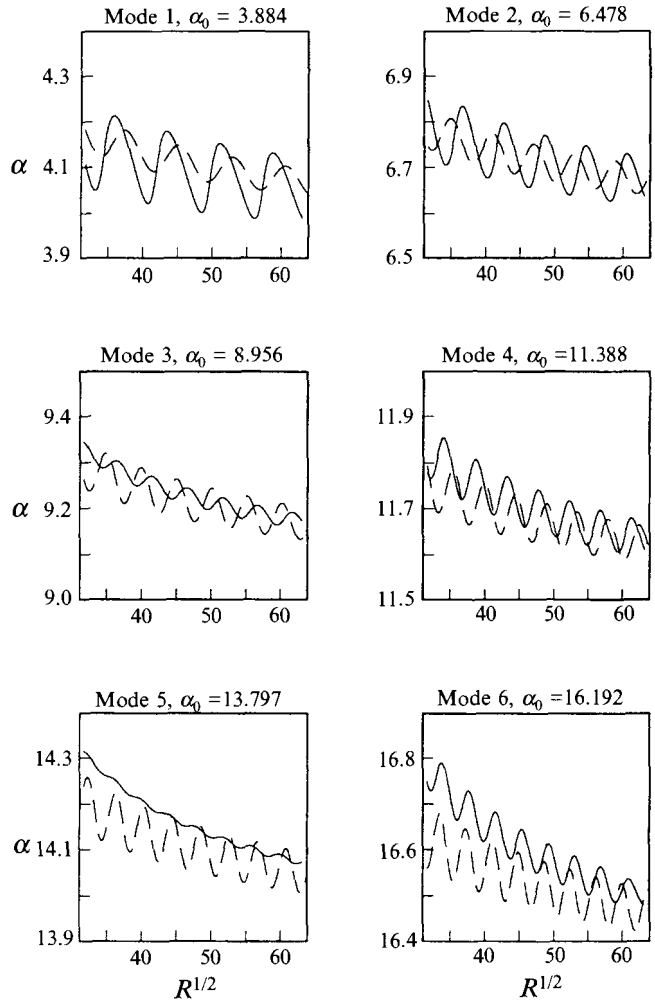

FIGURE 10. Eigenvalues for the long driven-cavity case: comparison between numerical (——) and asymptotic (– – –) $R \gg 1$ results, for $\alpha = O(1)$, $\mathrm{Re}(\alpha) > 0$ modes.

Eigenvalue	α_0	α_1	α_2	α_3
mode 1	3.8837	−0.3241	0.000	−4.5875
mode 2	6.4782	−0.4040	0.000	−5.7183
mode 3	8.9557	−0.4951	0.000	−7.0086
mode 4	11.3879	−0.5891	0.000	−8.3404
mode 5	13.7968	−0.6845	0.000	−9.6889
mode 6	16.1921	−0.7803	0.000	−11.0455

TABLE 4. Eigenvalues for the driven-cavity case

Rejecting, again, $\mathrm{Bi}(\zeta)$ as an unbounded solution to the problem, and applying the impermeability and no-slip boundary conditions for ϕ we obtain

$$\Phi_0 = \bar{C}_0 \int_0^{\zeta} \int_0^{\zeta_1} \mathrm{Ai}(\zeta_2)\, \mathrm{d}\zeta_2\, \mathrm{d}\zeta_1, \tag{109}$$

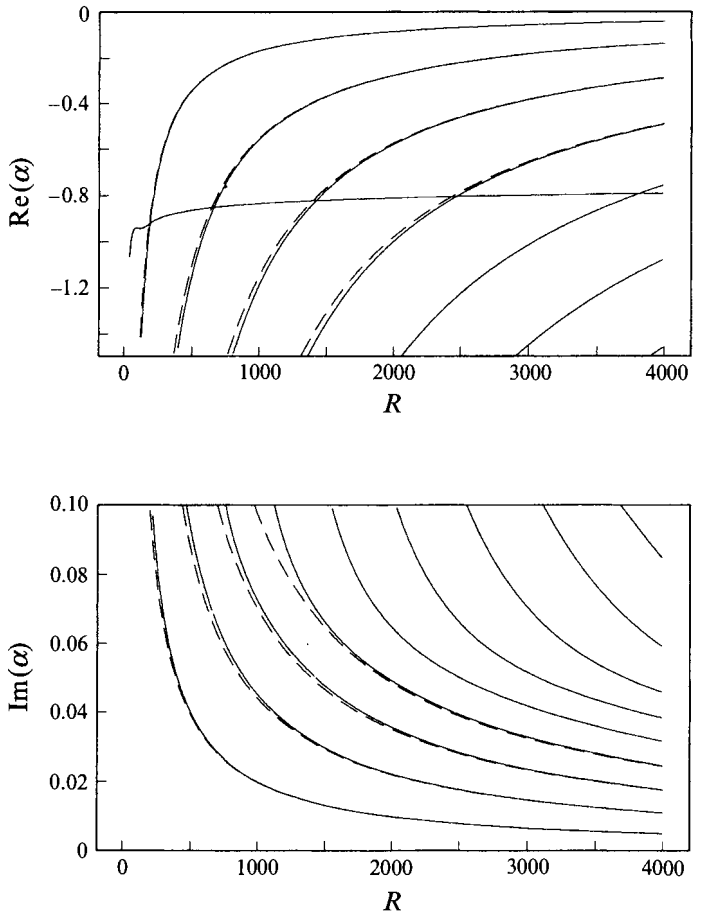

FIGURE 11. Complex eigenvalues for the long driven-cavity case, $\mathrm{Re}(\alpha) < 0$: comparison between numerical (——) and asymptotic (– – –) $R \gg 1$ results, for $\alpha = O(1/R)$ modes.

and so
$$\Phi_0 \to \tfrac{1}{3}\bar{C}_0\,\zeta + \bar{C}_0\,\mathrm{Ai}'(0) \tag{110}$$
in the limit as $\zeta \to +\infty$. Matching the inner and outer solutions implies $\bar{C}_0 = 3$ and this gives the boundary condition for ϕ_3 on $y = -1$.

The boundary conditions for the ϕ_i are as follows:
$$\phi_0(-1) = 0, \qquad \phi_0(\tfrac{1}{3}) = 0, \tag{111}$$
$$\phi_0'(-1) = 1, \qquad \phi_0'(\tfrac{1}{3}) = K, \tag{112}$$
$$\phi_1(-1) = 0, \qquad \phi_1(\tfrac{1}{3}) = (7/72\pi^{1/2})\,K, \tag{113}$$
$$\phi_2(-1) = 0, \qquad \phi_2(\tfrac{1}{3}) = 0, \tag{114}$$
$$\phi_3(-1) = 3\mathrm{Ai}'(0), \qquad \phi_3(\tfrac{1}{3}) = 0. \tag{115}$$

We are now in a position to solve (75) using adjoints. This leads immediately to $\alpha_2 = 0$ and
$$\alpha_i^2 = \frac{-\phi_i(-1)\,\phi^{\dagger\prime}(-1) + \phi_i(\tfrac{1}{3})\,\phi^{\dagger\prime}(\tfrac{1}{3})}{\displaystyle\int_{-1}^{\frac{1}{3}} \phi^\dagger \phi_0 \,\mathrm{d}y} \quad \text{for} \quad i = 1 \quad \text{and} \quad 3, \tag{116}$$
where $\phi^\dagger = \phi_0$, as before. The asymptotic representation for α takes the form
$$\alpha \sim \alpha_0 + \tfrac{1}{2}\cos\left((\alpha_0 R)^{1/2} I + \tfrac{1}{4}\pi\right)\alpha_1^2\,\alpha_0^{-5/4}\,R^{-1/4} + \tfrac{1}{2}\alpha_3^2\,\alpha_0^{-4/3}R^{-1/3} \quad \text{for} \quad \alpha_0 \neq 0. \tag{117}$$

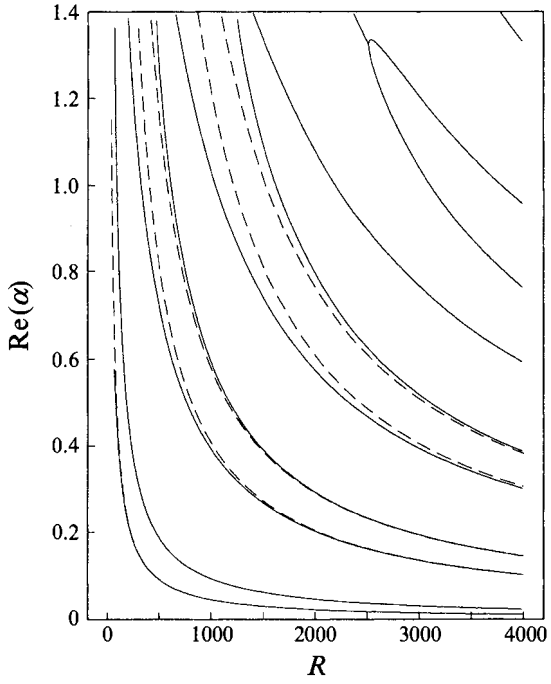

FIGURE 12. Eigenvalues for the long driven-cavity case, $\mathrm{Re}(\alpha) > 0$: comparison between numerical (——) and asymptotic (– – –) $R \gg 1$ results, for $\alpha = O(1/R)$ modes.

The numerical details are given in table 4, and a graphical comparison of the asymptotic (broken lines) and numerical values of α, over a range of $R^{1/2}$ is shown in figure 10; the comparison is encouraging. The qualitative features of these eigensolutions are also confirmed by the (fully) numerical results shown in figure 9, which indicates (relatively) low-frequency large-amplitude oscillations between $y = -1$ and $y \approx \frac{1}{3}$, and high-frequency small-amplitude oscillations between $y \approx \frac{1}{3}$ and $y = 1$.

6.2. $R \gg 1$, $\alpha = O(1/R)$ *modes*

For $R \gg 1$, two $O(1/R)$ eigenvalue families are found – one real family with $\mathrm{Re}(\alpha) > 0$, and one complex family with $\mathrm{Re}(\alpha) < 0$. If expansions (40) and (41) are substituted into (7), and terms of $O(1/R)$ are neglected, we obtain the equation

$$\phi_0^{\mathrm{iv}} + \tilde{\tilde{\alpha}}_0 \tfrac{3}{4}(y+1)(y-\tfrac{1}{3})\phi_0'' - \tfrac{3}{2}\tilde{\tilde{\alpha}}_0 \phi_0 = 0, \tag{118}$$

which can be solved numerically to give $\tilde{\tilde{\alpha}}_0$. Numerical results for the first few eigenvalues are given in table 2. Figure 11 shows a comparison between the numerical and asymptotic (dashed lines) results for the complex family of eigenvalues ($\mathrm{Re}(\alpha) < 0$, generally the $O(1/R)$ family, although one of the $O(1)$ modes is also perceptible). Figure 12 compares the numerical and asymptotic results (dashed lines) for the $\mathrm{Re}(\alpha) > 0$, $O(1/R)$ family of eigensolutions.

6.3. $R \gg 1$, $\alpha = O(1)$, $Re(\alpha) < 0$ *modes*

Only two members of the complex $O(1)$, $\mathrm{Re}(\alpha) < 0$ eigenvalue family were found. They are generated in a different manner to the $O(1)$ eigenvalues found for $\mathrm{Re}(\alpha) > 0$, and the two previous cases: the eigenvalues are solutions of (74) over the interval $y \in [-1, 1]$. Solving this equation numerically (using a Runge–Kutta approach) in this region causes problems due to the singularity in $\Psi_0'(y)$ at $y = \frac{1}{3}$. This difficulty

was circumvented by extending the solution into the complex y-plane to avoid the singularity. The two values of α thus obtained are $\alpha_0 \approx (-2.74, 0.77), (-0.71, 1.45)$. The variation of the second of these two modes at finite Reynolds number is to be seen on figure 11.

7. Conclusions

For low Reynolds numbers, the eigenvalues in all cases considered are complex, and indeed become independent of the base flow at $R = 0$, and generally undergo branching processes as the Reynolds number is increased. For higher Reynolds numbers, the eigenvalues found can be classified in terms of distinct eigenvalue families; these are summarized in table 5.

Asymptotic forms of the eigenvalue families have been described in all three cases. The asymptotic approximations have been compared to the solution of the full equations, and the correlation has, in general, been good. The validity of the numerical results obtained was confirmed by comparison with the results of Bramley & Dennis (1982), for the first case, and in all three cases the Runge–Kutta shooting method was used as an independent check.

Note that in the general situation it will be the eigenvalue of smallest wavenumber (i.e. longest wavelength) that persists furthest downstream/upstream, and so in the $R \to \infty$ limit will correspond to the $\alpha = O(1/R)$ family of eigenmodes. Nonetheless larger-wavenumber eigenmodes can still be important if disturbances of compatible scale are introduced into the flow. For example, a disturbance of streamwise extent $O(R^{-1/7})$ and transverse dimension $O(R^{-2/7})$ introduced close to either of the walls would trigger, predominantly, the $\alpha = O(R^{-1/7})$ modes described in this paper (see for example Smith 1982).

There are a number of fairly general observations to be made from table 5 regarding the nature of the eigenvalue families for $R \gg 1$. The $O(R^{-1/7})$ modes seem to be confined to the plane Poiseuille flow case, as confirmed in the Appendix, where it is seen that as the magnitude of the wall velocity increases, other modes form, and then the corresponding eigenvalues α either increase or decrease, presumably ultimately becoming members of the $\alpha = O(1)$ or $\alpha = O(1/R)$ families respectively.

The $\alpha = O(1)$ eigenvalues seem to be generally associated with upstream-decaying-type eigenmodes; these tend to be real eigenvalues and are physically/intuitively correct insofar as these eigenvalues indicate that the upstream effects as a result of these modes are felt only a distance $O(1)$ upstream (compared with a distance $O(R)$ downstream as a result of the $\alpha = O(1/R)$ family of eigenvalues). Notice that from our definition of basic flow, upstream-decaying modes correspond to $\mathrm{Re}(\alpha) > 0$ for plane Poiseuille flow, and $\mathrm{Re}(\alpha) < 0$ for the intermediate case; this 'inconsistency' in notation was chosen to obtain better consistency with the driven-cavity case.

The $\alpha = O(1/R)$ eigenvalues appear, on the whole, to be associated with downstream-decaying modes, which, generally fill the entire channel/cavity cross-section. Certainly, for $R \gg 1$, eigenvalues for the plane Poiseuille flow case and the intermediate case are all (with just one exception) real. On the other hand, the driven-cavity case is somewhat different in possessing (many) complex eigenvalues. However, this particular case is fundamentally different, since talk of 'upstream' or 'downstream' is misleading, due to the multi-directionality of the flow. In spite of this, for this case the $\mathrm{Re}(\alpha) > 0$, $\alpha = O(1)$ family of eigenvalues are real, and are of an interesting nature. They could be construed as being upstream-decaying modes, since these modes, to leading order, take on a predominately inviscid nature between the lower boundary,

Flow type	$\mathrm{Re}(\alpha) > 0$	$\mathrm{Re}(\alpha) < 0$
Poiseuille flow $\Psi_0'(y) = (y^2-1)$	$O(1)$ real eigenvalues $O(R^{-1/7})$ real eigenvalues	$O(1/R)$ real eigenvalues $O(R^{-1/7})$ complex eigenvalue
Intermediate case $\Psi_0'(y) = \frac{1}{4}(y+1)^2$	$O(1/R)$ real eigenvalues	$O(1)$ real eigenvalues
Driven-cavity case $\Psi_0'(y) = \frac{3}{4}(y+1)(y-\frac{1}{3})$	$O(1)$ real eigenvalues $O(1/R)$ real eigenvalues	$O(1/R)$ complex eigenvalues $O(1)$ complex eigenvalues

TABLE 5. Summary of eigenvalue families, for $R \gg 1$

and the point of flow reversal, and the wavenumbers to leading order are directly related to the $O(1)$ family of eigenvalues found in the case of plane Poiseuille flow. On the other hand, these eigenmodes take on a somewhat novel nature between the point of flow reversal and the upper boundary, being highly oscillatory, and very much dependent on viscosity. This suggests a highly nonlinear structure as the amplitude of the disturbance increases. This aspect is worthy of further attention, particularly because there seems to be every reason to suspect that this type of (eigensolution) behaviour would be a generic feature, applicable to many flows of this type at high Reynolds numbers. The $\mathrm{Re}(\alpha) < 0$, $\alpha = O(1)$ modes for the driven-cavity case seem quite different. We were able to find only two members of this family, and these eigensolutions fill the entire channel/cavity cross-section. There is some evidence that flow reversal causes eigenvalues to become complex, although the $O(1/R)$, $\mathrm{Re}(\alpha) > 0$ driven-cavity eigenmodes provide counter-examples to this. However, if we consider the solution of (118) in the limit as $\tilde{\tilde{\alpha}}_0 \to +\infty$, then we obtain the equation

$$(y+1)(y-\tfrac{1}{3})\phi_0'' - 2\phi_0 = 0, \tag{119}$$

which is, to leading order, the same equation as obtained for the $\mathrm{Re}(\alpha) > 0$, $\alpha = O(1)$ family of eigensolutions (equation (74)). Indeed, our numerical results (confirmed by asymptotic analysis very similar in detail to the $\alpha = O(1)$ analysis) indicate that as $\tilde{\tilde{\alpha}}_0 \to +\infty$, the eigenfunctions become progressively compressed into the region $-1 < y < \frac{1}{3}$. As a consequence, (119) leads to purely real solutions. In many ways, this similarity with the results for $\alpha = O(1)$ real eigenvalues is to be expected, on account of the 'overlap' that must occur when $\tilde{\tilde{\alpha}}_0 = O(R)$.

One final consideration here is the question of the stability of these classes of flow. As noted earlier, some aspects have been considered by Cowley & Smith (1985). However a number of possibilities exist, even though the basic flow profiles considered here are non-inflexional. One (strong) possibility, particularly relevant to our third class of basic flow, is that of absolute instability. This aspect will be the subject of further work. Additionally, three-dimensional effects would be of great interest.

The work of J.R.S. was supported by an EPSRC studentship. A number of computations were performed using computer facilities provided by EPSRC.

Appendix

We consider here the effect of a small boundary slip on the $\alpha = O(R^{-1/7})$ (defined in (39)) mode for the plane Poiseuille flow case of §4, in order to further confirm the general nature of the eigensolutions when flow reversal is present.

We suppose that the upper boundary has a slip $R^{-2/7}\hat{V}$, $\hat{V} = O(1)$. The process is

then similar to that of Wilson (1969) and Smith (1977). In the core the solution is expected to develop as

$$\phi = \phi_0 + R^{-2/7}\phi_1 + \ldots, \quad \Psi_0 = \psi_0 + R^{-2/7}\psi_1 + \ldots, \quad \alpha = R^{-1/7}\alpha_0 + \ldots, \tag{A 1}$$

where

$$\psi_0' = y^2 - 1, \quad \psi_1' = \tfrac{3}{4}\hat{V}(y+1)(y-\tfrac{1}{3}). \tag{A 2}$$

The governing equations are then

$$\mathrm{D}_4\phi_0 = 0, \quad \mathrm{D}_4\phi_1 = -\alpha_0^2\phi_0 - \phi_0''\frac{\psi_1'}{\psi_0'} + \phi_0\frac{\psi_1'''}{\psi_0'}, \tag{A 3a, b}$$

where

$$\mathrm{D}_4 \equiv \mathrm{d}^2/\mathrm{d}y^2 - 2/(y^2-1). \tag{A 4}$$

Equation (A 3*a*) has the exact solution

$$\phi_0 = \tilde{K}\psi_0', \tag{A 5}$$

which satisfies the required boundary conditions. When considering (A 3*b*), adjoint theory leads to the solvability condition

$$\phi_1(-1)\phi^{\dagger}(-1) - \phi_1(1)\phi^{\dagger}(1) = \tilde{K}^2[-\tfrac{16}{15}\alpha_0^2 - 2\hat{V}], \tag{A 6}$$

and, again, since (A 3*a*) is self-adjoint, $\phi^{\dagger} = \phi_0$, and by consideration of ϕ_0 near $y = \pm 1$ we obtain

$$\phi^{\dagger'}(-1) = -2\tilde{K}, \quad \phi^{\dagger'}(1) = 2\tilde{K}. \tag{A 7}$$

We also require the boundary conditions for ϕ_1. On $y = +1$, we consider the stretched coordinate $\eta = (1-y)R^{2/7}$ and the expansion for ϕ of the form

$$\phi \sim R^{-2/7}\hat{\phi}_0 + R^{-4/7}\hat{\phi}_1 + \ldots, \tag{A 8}$$

which gives

$$\hat{\phi}_0^{\mathrm{iv}} - 2\alpha_0(\eta - \tfrac{1}{2}\hat{V})\hat{\phi}_0'' = 0, \tag{A 9}$$

to leading order. Discarding the exponentially growing solution, this leads to

$$\hat{\phi}_0 = K_0\int_0^{\hat{\eta}}\int_0^{\hat{\eta}_1}\mathrm{Ai}(\hat{\eta}_2)\,\mathrm{d}\hat{\eta}_2\,\mathrm{d}\hat{\eta}_1 + K_1\hat{\eta} + K_2, \tag{A 10}$$

where K_0, K_1 and K_2 are constants, and $\hat{\eta} = (2\alpha_0)^{1/3}(\eta - \frac{1}{2}\hat{V})$ (noting $\eta \in \mathrm{Re}$ and $\eta > 0$). Since $\hat{\phi}_0(\eta = 0) = 0$, and $\hat{\phi}_0'(\eta = 0) = 0$, then

$$K_1 = K_0\int_0^{\hat{V}(2\alpha_0)^{1/3}/2}\mathrm{Ai}(-\hat{\eta}_2)\,\mathrm{d}\hat{\eta}_2 = K_0 A(\hat{V}) \tag{A 11}$$

and

$$K_2 = K_0[\mathrm{Ai}'(-\tfrac{1}{2}\hat{V}(2\alpha_0)^{1/3}) - \mathrm{Ai}'(0)] = K_0 B(\hat{V}). \tag{A 12}$$

To obtain boundary conditions for ϕ_1 on $y = 1$, we need to consider (A 10) (the inner solution) in the limit as $\eta \to \infty$ (to match with the outer solution). We find

$$\int_0^{\hat{\eta}}\int_0^{\hat{\eta}_1}\mathrm{Ai}(\hat{\eta}_2)\,\mathrm{d}\hat{\eta}_2\,\mathrm{d}\hat{\eta}_1 \to \frac{\hat{\eta}}{3} + \mathrm{Ai}'(0) \tag{A 13}$$

$$= \tfrac{1}{3}(2\alpha_0)^{1/3}\eta + \mathrm{Ai}'(0) - \tfrac{1}{2}\hat{V}\tfrac{1}{3}(2\alpha_0)^{1/3}. \tag{A 14}$$

Assuming $\arg(\alpha_0^{1/3}) \in (-\frac{1}{3}\pi, \frac{1}{3}\pi)$, (A 10) yields

$$\hat{\phi}_0 \to K_0[(A(\hat{V}) + \tfrac{1}{3})\hat{\eta} + \mathrm{Ai}'(0) + B(\hat{V})]. \tag{A 15}$$

By matching with the outer solution at $y = +1$, we obtain $K_0 = -2\tilde{K}/[(2\alpha_0)^{1/3}(A + \frac{1}{3})]$, and also

$$\phi_1(1) = \tilde{K}\hat{V} - 2\tilde{K}(\mathrm{Ai}'(0) + B(\hat{V}))/(2\alpha_0)^{1/3}(A(\hat{V}) + \tfrac{1}{3}). \tag{A 16}$$

The value of $\phi_1(-1)$ may be deduced from the above by setting $\hat{V} = 0$, to yield

$$\phi_1(-1) = -(6/(2\alpha_0)^{1/3})\,\mathrm{Ai}'(0)\,\tilde{K}. \tag{A 17}$$

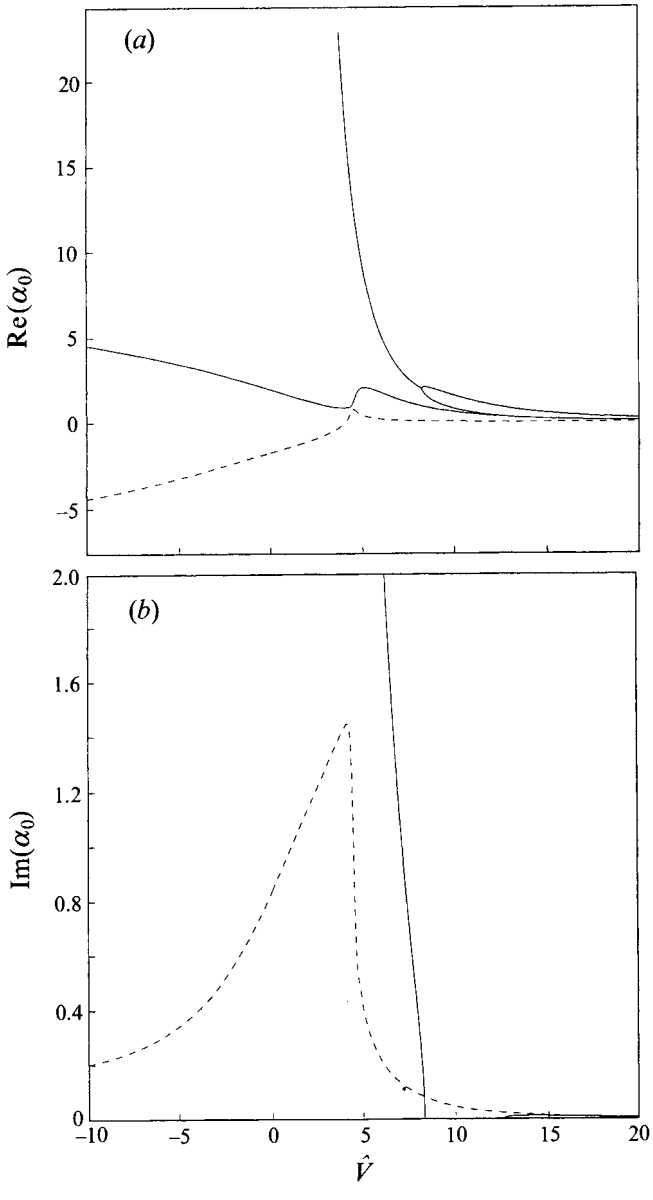

FIGURE 13. Variation of α_0 with $\hat{V}$; (*a*) Re(α_0), (*b*) Im(α_0).

The solvability condition yields the following dispersion relationship for α_0:

$$\frac{3\mathrm{Ai}'(0)}{(2\alpha_0)^{1/3}}+\frac{\mathrm{Ai}'(0)+B(\hat{V})}{(2\alpha_0)^{1/3}(A(\hat{V})+\frac{1}{3})}=-\tfrac{4}{15}\alpha_0^2. \tag{A 18}$$

Note that when $\hat{V}=0$, then $A(0)=B(0)=0$, and we obtain the plane Poiseuille flow results (effectively (39)), namely

$$\alpha_0=\tfrac{1}{2}[-90\mathrm{Ai}'(0)]^{3/7}, \quad \alpha_0=\tfrac{1}{2}\mathrm{e}^{6\mathrm{i}\pi/7}[-90\mathrm{Ai}'(0)]^{3/7}. \tag{A 19a, b}$$

The first of these corresponds to the complex (downstream) root of Wilson (1969), the second to the real (upstream) root of Smith (1977). Figure 13 shows the evolution of

the above two eigenvalues as $\hat{V}$ changes, with (A 19*a*) denoted by the broken line. Figure 13 does not represent *all* eigenmodes (but only the most important/slowly decaying), as detailed below. There are a number of important features observed in this figure, which we consider in turn.

Consider the limit $\hat{V}\to-\infty$; this turns out to be the simpler limit, with just the two original modes. Both values of $|\alpha_0|$ appear to grow in this limit. Our (numerical) results suggest (A 19*b*) remains real as $\hat{V}$ decreases, and that $A\to-\frac{1}{3}$ and $B\to-\mathrm{Ai}'(0)$. This being the case, utilizing the asymptotic form for the Airy function for large argument (which lies within the decaying segment of complex space), leads to

$$\alpha_0 \approx \tfrac{1}{2}\{-\tfrac{15}{2}\hat{V}\}^{1/2}. \tag{A 20}$$

As $\hat{V}\to-\infty$, the complex (downstream) root eigenvalue seems to have $A\to-\frac{1}{3}$, with B oscillating and growing (slowly). In this case, it appears that we have $\arg(\alpha_0)\to\pi$, and so the argument of the Airy function in this case approaches the limit of the decaying segment of complex space, and we deduce from (A 18) that

$$\alpha_0 \approx -\tfrac{1}{2}\{-\tfrac{15}{2}\hat{V}\}^{1/2}. \tag{A 21}$$

Let us now turn to consider $\hat{V}>0$. The situation is somewhat more complicated than before, due to the multiplicity of modes.

In addition to the modes (A 19), there exist additional modes which are unbounded as $\hat{V}\to0$. On figure 13, we have shown just a few of these modes, but in fact there seem to exist an infinity of modes. These modes do intersect, and at such points either a complex-conjugate pair of eigenvalues merge to form two distinct real modes, or alternatively two real modes merge to form a complex-conjugate pair; this type of behaviour is reminiscent of a number of results seen earlier in this paper.

Consider the limit now as $\hat{V}\to\infty$. Writing $\xi=(2\alpha_0)^{1/3}$, it appears that

$$\xi = \xi_0/\hat{V}+\ldots, \tag{A 22}$$

and so as $\hat{V}\to\infty$, we have

$$A\approx A_0=\int_0^{\xi_0/2}\mathrm{Ai}(-\hat{\eta}_2)\,\mathrm{d}\hat{\eta}_2, \quad B\approx B_0=\mathrm{Ai}'(-\tfrac{1}{2}\xi_0)-\mathrm{Ai}'(0). \tag{A 23}$$

Equation (A 18) then takes on the simplified form

$$3\mathrm{Ai}'(0)+(\mathrm{Ai}'(0)+B_0)/(A_0+\tfrac{1}{3})=0. \tag{A 24}$$

This system was solved numerically, and it turns out that there is an infinity of roots. The first five are $\xi_0\approx(4.8484,\pm1.3273)$, $(11.0432,\pm0.2474)$, $(15.5793,0)$, $(16.1929,0)$, $(19.7133,0)$. All additional roots appear to be real; these observations are entirely consistent with our numerical results for (A 18). Asymptotic analysis as $|\xi_0|\to\infty$ appears appropriate here; taking this limit leads to $\xi_0\approx2\{\frac{3}{2}\pi n\}^{2/3}$ as $n\to\infty$, indicating the infinity of modes.

As $\hat{V}\to0+$, consider now the behaviour of the additional (unbounded) modes. We retain our previous definition of ξ, but this time it develops in the following manner:

$$\xi = \xi_0/\hat{V}+\hat{V}^7\xi_1+\ldots. \tag{A 25}$$

We arrive at the following simplified dispersion relationship:

$$A\approx\int_0^{-\xi_0/2}\mathrm{Ai}(\eta)\,\mathrm{d}\eta=\tfrac{1}{3}. \tag{A 26}$$

The following are the first six roots to this equation:

$$\xi_0 \approx (13.5963,\ \pm 2.0632),\ (25.6682,\ \pm 1.7741),\ (35.3296,\ \pm 1.6265),$$
$$(46.4542,\ \pm 1.5038),\ (56.3704,\ \pm 1.4199),\ (65.47,\ \pm 1.3567).$$

Indeed, it would appear that there is an infinite number of these roots, since as $|\xi_0| \to \infty$, then

$$\xi_0 \approx -2\{\tfrac{3}{2}n\pi\}^{3/2} \tag{A 27}$$

as $n \to \infty$.

One further intriguing feature is to be seen in the results shown in figure 13(*a*). This concerns the region around $\hat{V} \approx 4.0163$, where the downstream root undergoes an important change, with $\mathrm{Re}(\alpha_0)$ changing sign. At this point, this particular mode changes its character, from being a downstream (oscillatory) mode to an upstream (oscillatory) mode, with directions referred to the direction of the main body of the flow. Indeed, this aspect is directly related to lower-branch (Tollmien–Schlichting) waves, which, in this context are non-travelling with respect to the lower (stationary) wall, but travelling with respect to the upper (non-stationary) wall.

We expect a breakdown of the above analysis when $\hat{V} = O(R^{2/7})$, in which case $\alpha = O(1)$, and the above analysis is no longer applicable.

REFERENCES

Bogdanova, E. V. & Ryzhov, O. S. 1983 Free and induced oscillations in Poiseuille flow. *Q. J. Mech. Appl. Maths* **36**, 271.

Bramley, J. S. 1984 Note on the calculation of eigenvalues for the stationary perturbation of Poiseuille flow. *J. Comput. Phys.* **53**, 524.

Bramley, J. S. & Dennis, S. C. R. 1982 The calculation of eigenvalues for the stationary perturbation of Poiseuille flow. *J. Comput. Phys.* **47**, 179.

Bramley, J. S. & Dennis, S. C. R. 1984 The calculation of eigenvalues for the stationary perturbation of Poiseuille flow using initial value methods. *J. Math. Anal. Applics.* **101**, 30.

Cowley, S J. & Smith, F. T. 1985 On the stability of Poiseuille flow: a bifurcation from infinity. *J. Fluid Mech.* **156**, 83.

Dennis, S. C. R. & Smith, F. T. 1980 Symmetrically constricted channel flows. *Proc. R. Soc. Lond.* A **372**, 393.

Duck, P. W. 1985 Laminar flow over unsteady humps. *J. Fluid Mech.* **160**, 465.

Moffatt, H. K. 1984 Viscous and resistive eddies near a sharp corner. *J. Fluid Mech.* **18**, 1.

Moler, C. B. & Stewart, G. W. 1973 An algorithm for generalized matrix eigenvalue problems. *SIAM J. Numer. Anal.* **10**, 241.

Orszag, S. A. 1971 Accurate solution of the Orr–Sommerfeld stability equation. *J. Fluid Mech.* **50**, 689.

Smith, F. T. 1977 Upstream interactions in channel flows. *J. Fluid Mech.* **79**, 631.

Smith, F. T. 1982 On the High Reynolds number theory of laminar flows. *IMA J. Appl. Maths* **28**, 207.

Stocker, J. R. 1992 Investigation of eigenvalues for the stationary perturbation of flow in a channel, including study of reversed flow. MSc thesis, University of Manchester.

Van Dyke, M. 1970 Entry flow in a channel. *J. Fluid Mech.* **44**, 813.

Wilson, S. D. R. 1969 The development of Poiseuille flow. *J. Fluid Mech.* **38**, 793.

Wilson, S. D. R. 1971 Entry flow in a channel. Part 2. *J. Fluid Mech.* **46**, 787.